Journal of Engineering Mathematics (2026) 158:4
https://doi.org/10.1007/s10665-026-10524-4

# Reactor-scale modelling and analysis of heat and mass transfer in silicon carbide rotary kilns

**Brady Metherall[1] · Ellen K. Luckins[2] · Alannah Neff[3] · Ferran Brosa Planella[2] · Colin P. Please[1]**

Received: 7 October 2025 / Accepted: 14 April 2026


**Abstract**
Silicon carbide is a widely used material due to its unique combination of physical and chemical properties. However, existing Acheson furnaces, which cause direct $CO_2$ emissions, are expensive and energy inefficient. Rotary kilns are a promising alternative, but their use for silicon carbide production is still under development. In this article, we present a mathematical model for the consumption of quartz and carbon, and the formation of silicon carbide in a rotary kiln. We focus on the interplay between reaction kinetics, solid and gas transport, and thermal effects. Assuming radial mixing within the bed, we derive a simplified one-dimensional model that captures the dominant physics of the system. The model tracks the evolution of quartz, carbon, and silicon carbide, as well as gas-phase species and temperature, down the length of the kiln. We nondimensionalise the model and identify key parameter groupings—relating supplied heat to kiln fill level, initial carbon particle size, and the relative speed of the two chemical reactions we consider. Then, we examine the model's behaviour via asymptotic analysis, before presenting numerical simulations. Our analysis shows that there is only one dimensionless parameter group that strongly influences reactor performance, with silicon carbide yield increasing monotonically with the value of this parameter. These findings offer broad-stroke insights into design principles and parameter operating regimes that favour efficient silicon carbide reactors.

**Keywords** Quartz–carbon systems · Reactive granular media · Rotary kiln modelling · Silicon carbide production · Solid–gas reactions

✉ Ellen K. Luckins
Ellen.Luckins@warwick.ac.uk

[1] Mathematical Institute, University of Oxford, Andrew Wiles Building, Radcliffe Observatory Quarter, Woodstock Road, Oxford OX2 6GG, UK

[2] Mathematics Institute, University of Warwick, Zeeman Building, Gibbet Hill Road, Coventry CV4 7AL, UK

[3] School of Mathematics, University of Edinburgh, James Clerk Maxwell Building, Peter Guthrie Tait Road, Edinburgh EH9 3FD, UK

Published online: 13 May 2026

## 1 Introduction

Silicon carbide (SiC) is a versatile material with a unique combination of thermal, mechanical, electronic, and chemical properties that make it valuable across a wide range of industrial applications. Its high melting point, excellent thermal conductivity, and hardness [1] enable its use in high-temperature environments and abrasive components such as grinding discs. As a wide-bandgap semiconductor, silicon carbide also plays a central role in high-power, high-temperature electronic devices [2]. Its chemical inertness, high melting point, and thermal conductivity have also led to its adoption as a structural material in demanding environments, such as nuclear fusion reactors [3]. In biomedical engineering contexts, silicon carbide is bio- and hemo-compatible, meaning it can be implanted without causing inflammation, toxicity, disrupting biological processes, or requiring additional sealants. Combined with its electronic functionality and durability, silicon carbide is a leading candidate for long-term implantable devices [4]. Finally, silicon carbide is emerging as a promising material for integrated quantum photonic technologies [5].

Silicon carbide is traditionally produced using the Acheson method [6], which is both energy intensive and chemically inefficient, as a lot of silicon escapes the furnace as silicon monoxide [7]. Given its growing role in advanced technologies, designing reactors for more efficient and scalable production of silicon carbide has become an active area of industrial research. There is growing interest in developing mathematical models and numerical tools to support design and control strategies.

The methods above are primarily focussed on creating silicon carbide in the alpha phase. Here, we concentrate on the earlier process of creating silicon carbide in the beta phase, which involves reactions between quartz ($SiO_2$) and carbon (C) at temperatures around 1750 °C. The heat treatment necessary to convert beta to alpha will not be considered. Specifically, the dominant reactions are

$$\mathrm{SiO_2}(s) + \mathrm{C}(s) \rightarrow \mathrm{SiO}(g) + \mathrm{CO}(g), \quad \Delta H = 792 \times 10^3 \ \mathrm{J/mol}, \tag{1}$$

which consumes quartz and carbon, and generates silicon monoxide (SiO) and carbon monoxide (CO), and

$$\mathrm{SiO}(g) + 2\,\mathrm{C}(s) \rightarrow \mathrm{SiC}(s) + \mathrm{CO}(g), \quad \Delta H = -78 \times 10^3 \ \mathrm{J/mol}, \tag{2}$$

which converts the silicon monoxide to silicon carbide. There is uncertainty over how physically realistic reaction (1) is since it is a solid–solid reaction. It is more likely that reaction (1) proceeds through intermediary gas reactions via carbon monoxide and carbon dioxide [8]. However, here, we consider the simplified chemistry of the solid–solid reaction following [9–12]. This is justified since, at the relevant temperature range, the second intermediary gas reaction is significantly faster than the first [13], and thus it is common to approximate the process by the overall solid–solid reaction (1). Among these two reactions (1)–(2), reaction (1) is typically slower, and the rate-limiting step of silicon carbide production. Consequently, the two reactions are sometimes "added

together" and treated as the single net process

$$\mathrm{SiO_2}(s) + 3\,\mathrm{C}(s) \rightarrow \mathrm{SiC}(s) + 2\,\mathrm{CO}(g), \quad \Delta H = 714 \times 10^3\ \mathrm{J/mol}, \tag{3}$$

which has been widely studied [8, 13–17].

In any silicon carbide reactor, the physical processes of heat transfer, solid–solid contact, evolution of the surface area of reactants, and gas flows strongly affect the chemical process. Understanding silicon carbide production therefore requires both theoretical modelling and detailed experimental investigation. Modelling provides insight into the interplay between reaction kinetics, gas transport, and heat transfer, but the dynamics are sensitive to the estimates of parameter values. Experimental work is essential to identify which chemical reactions are dominant under given operating conditions, and to measure their rate constants, activation energies, and enthalpies. This information is crucial for developing predictive models and for designing efficient reactors.

Early experimental studies, such as those by Wiik [18], provide foundational insight into the chemical mechanisms involved in quartz–carbon systems. Subsequent experiments have explored different material configurations and temperature ranges.

Various preprocessing of the raw quartz and carbon have been examined, which change the quartz–carbon contact surface area and the dynamics of the gas flow. For instance, the raw materials might be formed into pellets in which a porous carbon layer is chemically deposited on a quartz core, or transformed into bound agglomerates of finely ground quartz and carbon particles [19, 20]. Alternatively, the materials might be used in the simple form of fine individual particles of quartz and carbon. Each approach presents different advantages and challenges for efficiency, reactivity, mechanical integrity, and manufacturability.

Weimer et al. [11], and Agarwal and Pal [13] performed rapid-heating studies on agglomerates, observing the formation and escape of silicon monoxide gas under various carbon loadings and particle sizes. More recently, Li [19] compared carbon-coated quartz pellets with agglomerates formed from different carbon sources. His results demonstrated the importance of particle morphology, composition, and carbon reactivity, and confirmed that high silicon carbide yield depends not only on thermodynamics, but also on gas-phase retention and surface reactions. These studies demonstrate the need for well-designed experiments that match the relevant temperatures, pressures, and geometries of proposed reactor operations.

It is not yet clear which configuration of feed quartz and carbon is optimal for maximising silicon carbide yield. This uncertainty in raw material design, along with the difficulty of *in situ* measurements at high temperatures, motivates the development of mathematical models to better understand and predict the system dynamics. Modelling allows one to explore the coupled influences of chemical kinetics, gas transport, and heat transfer across reactor configurations and parameter ranges, and to investigate how these processes interact with evolving material geometries. Moreover, up-scaling from pilot- or laboratory-scale experiments to full industrial reactors introduces additional challenges. The interplay between transport and reaction kinetics may not scale linearly with size. Mathematical models provide a valuable tool for predicting how these factors vary with scale and help inform reactor design and operation in indus-

trial settings. Alongside experimental efforts, mathematical modelling has played a key role in interpreting data and exploring experimental set-ups that are difficult or expensive to realise.

Particle- and laboratory-scale models have been proposed to capture the essential dynamics of silicon carbide systems. These include a single-pellet model that resolve the interplay between diffusion and reactions in carbon-coated quartz particles [21]. The balance between diffusion and reaction (2) was shown to be key. If silicon monoxide quickly diffuses through the carbon layer it is lost to the external environment. Multiphase models have also been used to track the evolution of carbon, quartz, silicon carbide, and gas in an *isothermal* packed bed [22]. The effect of transport on the silicon carbide yield was less significant than for the pellets. Instead, the key balance was between the chemical reactions. Reaction (2) must be fast to achieve a high silicon carbide yield, but a side reaction must be slow to maintain safe operating gas pressures. A simplified one-dimensional laboratory-scale crucible furnace model focusing on the thermal dynamics was developed at the 171st European Study Group with Industry [23]. Their results highlighted the importance of gas residence time and venting in determining reactor efficiency.

Laboratory-scale crucible tests in induction furnaces indicate challenges with heat transfer and heat penetration in packed beds. We note that reaction (1) is endothermic. Once the outer region of the crucible is hot enough for reaction (1), any additional heat is consumed by the reaction instead of heating the inner region. Thus, we find that the reaction proceeds inward from the outer wall. This is undesirable for two reasons. First, the process becomes very time consuming—and potentially unfeasible on an industrial-scale. Second, while the conversion is happening in the inner region, the outer silicon carbide will continue to heat. Increasing temperature may increase the probability of silicon metal production, which is not desired.

We are therefore motivated to consider a horizontal rotary kiln, in which the rotation induces motion of the granular bed. Ideally, the rotation promotes mixing of the granular material, thereby increasing the uniformity of heating and reduced thermal gradients within radial cross-sections. Rotary kilns are widely used in metallurgy for processes including drying, incineration, calcination and reduction reactions [24], but they have not previously been used for silicon carbide production.

For existing rotary kiln applications, gaseous reactants (e.g. oxygen) are abundant and so rarely tracked explicitly, and gases produced are typically waste products, so that gaseous losses are not important. Moreover, the chemical reactions in rotary kilns are usually exothermic. Conversely, for a silicon carbide rotary kiln, the chemical process is strongly endothermic, and losses of the gaseous silicon monoxide must be limited as this results in chemical inefficiency. Indeed, the potential for significant silicon monoxide losses in the rotary kiln set-up is an important concern in developing this silicon carbide production method, and requires detailed investigation.

Acheson furnaces predominantly produce $\alpha$-SiC, whereas rotary kiln processes are designed to produce $\beta$-SiC. Compared with Acheson furnaces, the rotary kiln's enhanced heat transfer requires lower energy inputs to trigger the reactions, and its long and thin geometry, open only at the ends, allows for longer residence times of the silicon monoxide, which can potentially lead to lower silicon losses. However,

the main current challenge regarding silicon carbide rotary processing is whether the design and operation parameters are realistic for an industrial-scale setup.

Mathematical modelling is a very valuable tool to assess the viability of process. Existing models of rotary kilns typically focus on the granular flow of solid and heat transfer within the solid bed of the kiln [24]. Therefore, new models are required to understand these atypical characteristics of a silicon carbide rotary kiln; to our knowledge, no such models for silicon carbide rotary kilns have yet been proposed.

In this paper, we present the first model for a silicon carbide rotary kiln. We aim to capture the important processes in a simplest possible model, to give broad-strokes insight and thus to guide future experimental exploration of this potential silicon carbide-production process. In particular, the novelty of the rotary-kiln design compared to other silicon carbide-production processes is the significant heat transfer within the bed due to the mixing induced by the rotating flow. We assume that the bed is well mixed, so that the temperature and composition only varies along the length of the kiln and in time. We also make some simplifying assumptions about the granular flow and chemical reactions. The key mechanisms captured and elucidated by our model are the coupled thermal, chemical, and flow processes through the rotary kiln.

In the remainder of the paper, we derive a one-dimensional model under the assumption that cross-sections of the bed are well mixed in Sect. 2. The model couples reaction rates, solid and gas evolution, and thermal transport. We then nondimensionalise the model in Sect. 3. We proceed by examining the asymptotic structure of the problem in Sect. 4, and numerical solutions in Sect. 5. Finally, in Sect. 6, we summarise our findings and provide possible avenues of future work.

## 2 Model of solid flow, heat transfer, and reaction kinetics in a rotary kiln

We consider a simplified model for the distribution of heat and chemical species in a rotary kiln, which is affected by the motion of the granular solid, the flow of gas, and the chemical reactions. We take a highly idealised view with the aim of giving insight into the dominant trends in the behaviour.

In particular, we will assume that the granular bed is well mixed due to the rotational motion. We adopt this assumption based on prior studies that have demonstrated strong cross-sectional mixing in rotary kilns. This means that our operating conditions fall within the tumbling regime (see Table 1 in [25]), which is the typical regime for rotary kilns. The regime depends mainly on the friction coefficient between the material and the kiln, the filling fraction, and the rotating speed. However, as a rule of thumb, we expect the tumbling regime to be at intermediate rotation speeds: too low of a speed, and the kiln operates in the slipping regime, while too high of a speed and the kiln operates in the centrifuging regime (it is not immediately obvious what would happen in the cataracting regime). In either case, mixing will be limited and therefore the heat transfer will be restricted by conduction through the particles, and thus too slow, thereby creating thermal and reaction rate gradients through the bed. In the tumbling regime, we anticipate the motion of particle to be sufficiently rapid that the time for

particles to circulate in the bed is small compared to the time for any significant change in temperature or reaction rate along the furnace so that good mixing occurs.

Numerical simulations using computational fluid dynamics, the discrete element method, two-fluid models, and quasi-three-dimensional models show effective radial homogeneity of temperature [26–29]. Owens et al. [30] combined pilot-scale experiments with a heat transfer model, and conclude that the assumption of a well-mixed, radially isothermal bed is appropriate under the conditions they tested. Namely, rotation rates of 0.1–1 rpm, fill fractions of 3–8%, and residence times of 5–45 min—conditions that we anticipate to align with the operation of our system.

Hence, we will assume that the spatial distribution of the chemical species in the bed is uniform in each cross-section. The volume fraction of the solid chemical species of the bed, the gas concentrations, and the temperature of the solid and the gases in the bed equilibrate quickly in any cross-section, and so they are uniform.

Our model will not explicitly distinguish between the different preprocessings of feed material described in Sect. 1. We note that in each case the particle-to-kiln diameter ratio is small. Although the internal transport dynamics within each form will differ—carbon-coated quartz pellets impose longer diffusion lengthscales, agglomerates provide shorter diffusion paths, and fine particles attempt to maximise surface area—the bulk behaviour we will model is broadly applicable. Fluidisation is unlikely to occur for the larger pellets or agglomerates, but may be a concern for finely ground individual particles. We proceed under the assumption that the granular bed does not become fluidised.

The next assumption is that gas pressure variations are small. Large amounts of gaseous products are produced in the reactions, and so in practice, we anticipate the kiln will be open to the atmosphere at the ends, allowing a free flow of the gases in the channel. Hence, we will make the approximation that the total gas pressure everywhere is near atmospheric pressure. This assumption will greatly simplify the model, since, when combined with the one-dimensional nature of the model, the near-constant gas pressure replaces the need to consider conservation of momentum in the gas. The conservation of species will determine the motion of the gas and the motion will create the small pressure variations necessary to balance momentum.

In Fig. 1, the basic structure of the problem is outlined. We use $x$ as the coordinate down the kiln with the solids in the bed moving at net speed $u$ in the $x$-direction, and with a cross-sectional area of $A$. In the bed, we have three solid species and we quantify the amount of each solid using the volume fraction (within the bed volume) $S_i$ of each solid species, where $i \in \{\mathrm{SiO_2}, \mathrm{C}, \mathrm{SiC}\}$ are the relevant species. In the bed, we also consider two gases moving in the pore space, which has porosity $\phi$, and quantify them using their intrinsic gas concentration (within the void volume) $G_i$, where $i \in \{\mathrm{SiO}, \mathrm{CO}\}$ are the relevant gas species. We now proceed to derive the governing equations by considering conservation of the various species and some basic physical properties. We anticipate three regions to exist within the kiln, the pre-heating zone, the hot zone, and the post-reaction zone (see Fig. 1). In the pre-heating zone the solid materials must be heated up to an appropriate temperature for the reactions to begin. The consumption of the quartz and carbon, and production of silicon carbide will happen within the hot zone. Lastly, if we exhaust the quartz before reaching the

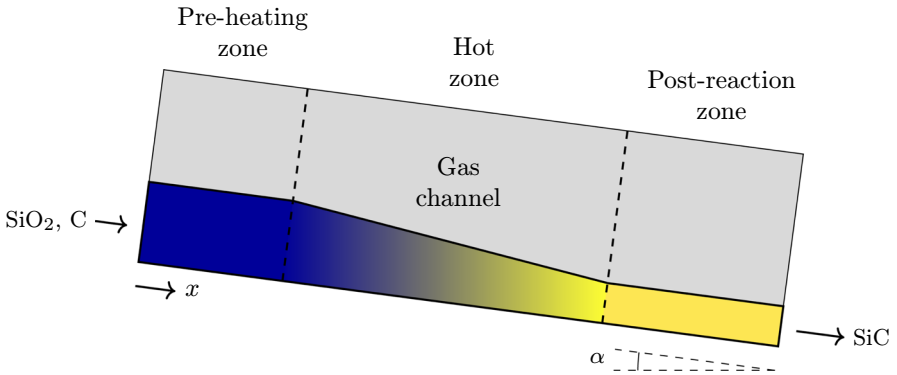


**Fig. 1** Cross-section of a silicon carbide rotary kiln reactor. The kiln is divided into three axial zones: a pre-heating zone, a hot reaction zone, and a post-reaction zone. The granular bed (blue and yellow, illustrating the composition of solid reactant/product) is assumed to be well mixed in each cross-section due to kiln rotation. Within the hot zone, conversion of quartz and carbon (blue) into silicon carbide (yellow) occurs. A gas channel (grey) lies above the bed, which allows the removal of gaseous products such as carbon monoxide. We do not model the gas channel explicitly, since gases are assumed to be lost from the granular bed to the channel via a one-way coupling only. The angle $\alpha$ denotes the kiln's inclination, which, in combination with rotation, drives the axial transport of solids

outlet of the reactor, we will have the post-reaction zone. In this zone no reactions take place since we have consumed all of our key reactant.

### 2.1 Granular bed

We start the modelling by considering the various physical processes in the bed and present conservation laws that account for these mechanisms. Conservation of quartz, carbon, and silicon carbide take the form

$$\frac{\rho_{\mathrm{SiO_2}}}{M_{\mathrm{SiO_2}}}\left(\frac{\partial}{\partial t}\left(AS_{\mathrm{SiO_2}}\right)+\frac{\partial}{\partial x}\left(AS_{\mathrm{SiO_2}}u\right)\right)=-Ar_1, \tag{4}$$

$$\frac{\rho_{\mathrm{C}}}{M_{\mathrm{C}}}\left(\frac{\partial}{\partial t}\left(AS_{\mathrm{C}}\right)+\frac{\partial}{\partial x}\left(AS_{\mathrm{C}}u\right)\right)=-A(r_1+2r_2), \tag{5}$$

$$\frac{\rho_{\mathrm{SiC}}}{M_{\mathrm{SiC}}}\left(\frac{\partial}{\partial t}\left(AS_{\mathrm{SiC}}\right)+\frac{\partial}{\partial x}\left(AS_{\mathrm{SiC}}u\right)\right)=Ar_2, \tag{6}$$

respectively, where $\rho_i$ denotes the bulk density and $M_i$ the molar mass of each solid phase (the volume fractions $S_i$, cross sectional area $A$, and velocity $u$ are as defined in the previous section). Here $r_1$ and $r_2$ are the two reaction rates of reactions (1) and (2) with units of $[\mathrm{mol\,m^{-3}\,s^{-1}}]$. We will specify their functional form shortly.

We might expect the rate of reaction (2) to depend on the available surface area of carbon. To capture this effect, we introduce the number density of carbon particles $n_{\mathrm{C}}$ into the model. Note that just the volume fraction of carbon is insufficient (the packing fraction of spheres is independent of particle size, and hence, surface area). Alternative parametrisations, such as particle radius or surface area explicitly, are possible but

give less convenient conservation equations. In our formulation, the number of carbon particles is conserved. Accordingly, the conservation law is

$$\frac{\partial}{\partial t}\left(An_{\mathrm{C}}\right)+\frac{\partial}{\partial x}\left(An_{\mathrm{C}}u\right)=0. \tag{7}$$

Conservation of silicon monoxide and carbon dioxide (with concentrations $G_i$, as above) yield

$$\frac{\partial}{\partial t}\left(\phi AG_{\mathrm{SiO}}\right)+\frac{\partial}{\partial x}\left(\phi AG_{\mathrm{SiO}}u\right)+FG_{\mathrm{SiO}}=A(r_1-r_2), \tag{8}$$

$$\frac{\partial}{\partial t}\left(\phi AG_{\mathrm{CO}}\right)+\frac{\partial}{\partial x}\left(\phi AG_{\mathrm{CO}}u\right)+FG_{\mathrm{CO}}=A(r_1+r_2), \tag{9}$$

where we have introduced the volume flux of gas out of the bed and into the gas channel, $F$. We anticipate that because the bed is very long and thin the gas velocity (within the bed) will be very close to $u$. Owing to the significant aspect ratio, the large volumes of gas produced will preferentially flow through the channel, rather than the porous bed. We therefore assume the solid and gas move down the kiln at the same speed, and use $u$ from here on for the gas velocity as well.

Having quantified the solids using their volume fractions, we know that adding up all the species must give unity, so we have

$$S_{\mathrm{SiO_2}}+S_{\mathrm{C}}+S_{\mathrm{SiC}}+\phi=1. \tag{10}$$

We assume that the gas satisfies the ideal gas law *and* that the pressure is atmospheric pressure everywhere. Hence, we write

$$P_a=\left(G_{\mathrm{SiO}}+G_{\mathrm{CO}}\right)RT \tag{11}$$

where $T$ is the temperature in the bed, $R$ is the universal gas constant, and $P_a$ is atmospheric pressure.

We now consider thermal transport mechanisms within the bed. Since the pores are very small in the bed, we assume the gas to be at the same temperature as the solid, $T$. We will assume that there is some bulk heating $Q(x,t)$ that is externally prescribed. This may be the prescribed heat flux applied to the rotary kiln at position $x$ from an induction source, a flame, a plasma torch, or another source. When considering conservation of heat we should balance advection in the solid, advection in the gas, heat loss to the gas channel, the external heat source, and heats of reaction so that

$$\begin{aligned}\frac{\partial}{\partial t}\left((1-\phi)\rho_S c_S AT\right)+\frac{\partial}{\partial x}\left((1-\phi)\rho_S c_S ATu\right)+\frac{\partial}{\partial t}\left(\phi\rho_G c_G AT\right)\\ +\frac{\partial}{\partial x}\left(\phi\rho_G c_G ATu\right)=-F\rho_G c_G T+Q-A\sum_j \Delta H_j r_j.\end{aligned} \tag{12}$$

Here we have introduced the notation for the density of the gas $\rho_G = M_{\mathrm{SiO}} G_{\mathrm{SiO}} + M_{\mathrm{CO}} G_{\mathrm{CO}}$ and the specific heats of the solid $\rho_S c_S = \sum_i \rho_i c_i S_i$ and the gas $\rho_G c_G = M_{\mathrm{SiO}} c_{\mathrm{SiO}} G_{\mathrm{SiO}} + M_{\mathrm{CO}} c_{\mathrm{CO}} G_{\mathrm{CO}}$. We have also introduced the heat of reaction ($\Delta H_j$) for the two reactions. Note that we have assumed that the gas is leaving the bed and entering the gas channel so the temperature used for this transfer is the bed temperature. Finally, we observe that the density of the gas is much less than that of the solid, so we simplify (12) to

$$\begin{aligned} \frac{\partial}{\partial t}\left((1-\phi)\rho_S c_S A T\right) + \frac{\partial}{\partial x}\left((1-\phi)\rho_S c_S A T u\right) \\ = -F\rho_G c_G T + Q - A\sum_j \Delta H_j r_j. \end{aligned} \tag{13}$$

As the particles in the bed react, the granular material will rearrange itself. Rather than considering momentum in any way explicitly, we assume the very simple law that the bed compacts quickly and retains a constant porosity

$$\phi = \phi_0. \tag{14}$$

Therefore, the cross-sectional area $A$ of the bed changes spatially and in time. We note that other compaction laws are possible when the momentum of the granular flow is explicitly modelled, see for example [31–33]. There are also alternative modelling choices which would remove the requirement for explicitly modelling the granular bed flow, such as requiring the bed cross-sectional area $A$ remains constant (and so the porosity increases). This was done in [34], for instance. However, for the present rotating kiln, it is much more realistic to assume that the particles easily rearrange to maintain a constant porosity.

We assume that we know some quasi-static relationship between the cross-sectional area of the bed $A$ and the solid velocity $u$, in terms of system parameters such as kiln rotation speed $\omega$, inclination angle $\alpha$, friction properties of the particles, *etc*. Hence, there is some known (perhaps empirical) function $f$ satisfying

$$f(u, A; \omega, \alpha, \dots) = 0, \tag{15}$$

that governs the solid flow in the kiln. Specific choices for $f$ are discussed in Sect. 4 below.

### 2.2 Gas channel

We do not model the gas channel explicitly, as it is not expected to influence the behaviour of the bed. First, the density of the gas is several orders of magnitude smaller than that of the solid phase, so even substantial variations in gas composition or temperature correspond to comparatively negligible amounts of mass and energy. Second, the contact area between the gas channel and the bed is small. This limits the potential for heat exchange across the interface. Our previous modelling is consistent

with the assumption that the dynamics within the gas channel do not affect the temperature, composition, or reaction rates in the bed. Including the gas channel in the model would therefore add complexity without changing the predicted behaviour of the bed. We thus restrict our attention to the bed alone.

In other silicon carbide and silicon production processes, recapture of the silicon from the silicon monoxide gas is achieved by condensation reactions as the gases are forced to flow through a porous bed of cold reactants. This recapture mechanism is expected to be much less significant in the rotary kiln, due to the small solid–gas surface area as described above, and thus it is neglected from our model. We discuss how our model might be extended to include such condensation reactions in the conclusions section.

### 2.3 Reaction kinetics

We now discuss the form of the reaction rates $r_1$ and $r_2$. Despite extensive investigation, the reaction kinetics are not well understood [18]. First, $r_1$ is associated with reaction (1). Although the two reactants are solid, it is reasonable to assume that the dynamics of the process are similar to that involving two gases, where the law of mass action is applicable. This reaction is known to be sensitive to temperature variations in the regime of interest and so we adopt the usual Arrhenius rate dependence on the bed temperature. We therefore take the model of the kinetics to be

$$r_1 = k_1 \mathrm{e}^{-E_1/RT_B} S_{\mathrm{SiO_2}} S_{\mathrm{C}}, \tag{16}$$

where $k_1$ is the associated rate constant and $E_1$ is the activation energy.

For $r_2$, the reaction (2) is between a gas and a solid, and it is known that the resulting product creates a porous silicon carbide layer on the carbon particle that the gaseous silicon monoxide must diffuse through to get to the unreacted carbon surface. Various detailed models exist to describe this diffusive behaviour [35–37], and the reduction of the carbon surface as the particle is turned to silicon carbide [11]. In the interest of enabling easy interpretation of the results we make a simple approximation.

One model of the kinetics is to assume the particle volume is consumed uniformly across its surface. We assume the reaction rate is proportional to the surface area of carbon, and model the kinetics as in [22]. For particles with characteristic radius $r$, the surface area per volume, $a$, and volume fraction, $S$, scale as

$$a \propto r^2 n, \quad S \propto r^3 n, \tag{17}$$

so that

$$r \propto \left(\frac{S}{n}\right)^{1/3}, \tag{18}$$

and thus,

$$a \propto \left(nS^2\right)^{1/3}. \tag{19}$$

We now need to address the change in $r_2$ with temperature. In principle, this reaction could also be modelled with Arrhenius-type kinetics. However, over the temperature range of interest, its effective temperature sensitivity is expected to be weak relative to that of $r_1$. Experimental observations indicate that silicon monoxide is initially consumed rapidly, with reaction (2) proceeding quickly until transport limitations arise within the porous product layer [18]. We neglect any explicit temperature dependence and write

$$r_2 = k_2 \left(n_{\mathrm{C}} S_{\mathrm{C}}^2\right)^{1/3} \phi_0 G_{\mathrm{SiO}}, \tag{20}$$

by the law of mass action, where $k_2$ is the associated rate constant, independent of $T$.

### 2.4 Model structure, boundary, and initial conditions

The model (4)–(11) and (13)–(15) presented above is a closed system of 11 equations for the 11 unknowns

$$S_{\mathrm{C}}, \quad S_{\mathrm{SiO2}}, \quad S_{\mathrm{SiC}}, \quad n_{\mathrm{C}}, \quad G_{\mathrm{SiO}}, \quad G_{\mathrm{CO}}, \quad A, \quad F, \quad T, \quad \phi, \quad u. \tag{21}$$

The model couples four algebraic constraints, (10), (11), (14), and (15), with seven conservation laws, (4)–(9) and (13), all of which are first-order hyperbolic equations with the same characteristics following the motion of material down the kiln. We assume that the bed is always travelling in the positive $x$-direction ($u > 0$). For each of these hyperbolic equations it appears that we require both an initial condition, at $t = 0$, and a boundary condition at the inlet of the kiln, $x = 0$. Since we will be most interested in the steady-state operation of the kiln, we focus on the boundary conditions at $x = 0$. At $t = 0$ we will assume that the kiln is uniform, with variables taking the same values as the inlet conditions (as if the kiln has been running indefinitely without heating applied).

Given the constant porosity constraint (14), we view (4)–(6) and (10) as equations for $S_{\mathrm{SiO2}}$, $S_{\mathrm{C}}$, $S_{\mathrm{SiC}}$, and $A$. In particular, summing the three conservation laws (4)–(6) and making use of (10) we obtain

$$\frac{\partial A}{\partial t} + \frac{\partial}{\partial x}(Au) = \frac{A}{1-\phi_0}\left(-\frac{M_{\mathrm{SiO2}}}{\rho_{\mathrm{SiO2}}} r_1 - \frac{M_{\mathrm{C}}}{\rho_{\mathrm{C}}}(r_1 + 2r_2) + \frac{M_{\mathrm{SiC}}}{\rho_{\mathrm{SiC}}} r_2\right), \tag{22}$$

a hyperbolic equation for $A$. Since the reaction kinetics are independent of $S_{\mathrm{SiC}}$, it is convenient to use the conservation laws (4), (5), and (22) for $S_{\mathrm{SiO2}}$, $S_{\mathrm{C}}$, and $A$, and to view (10) as an equation for $S_{\mathrm{SiC}}$. We therefore require the boundary conditions

$$A = A_0, \quad S_{\mathrm{SiO2}} = S_{\mathrm{SiO2}}^0, \quad S_{\mathrm{C}} = S_{\mathrm{C}}^0 \quad \text{at } x = 0 \text{ (and at } t = 0). \tag{23}$$

Specifically, we assume that the only solid materials added to the kiln at the inlet are quartz and carbon, so that

$$S^0_{\mathrm{SiO_2}} + S^0_{\mathrm{C}} = 1 - \phi_0, \tag{24}$$

at $x = 0$, by (10). Under the assumption of a high operational efficiency, the inlet solid composition must be set by the stoichiometric balance of the net chemical reaction (3), so that

$$3\frac{\rho_{\mathrm{SiO_2}}}{M_{\mathrm{SiO_2}}} S^0_{\mathrm{SiO_2}} = \frac{\rho_{\mathrm{C}}}{M_{\mathrm{C}}} S^0_{\mathrm{C}}. \tag{25}$$

This corresponds to a feed mixture in which quartz and carbon are present in the proportions required for complete reaction, consistent with maximising silicon carbide yield under ideal conditions. While a small excess of carbon is desirable for silicon carbide yield, deviations from a stoichiometric inlet composition towards carbon- or quartz-rich feeds lead to residual excess reactant in the feed [38]. Such residuals are undesirable as, at least in the case of carbon, they are difficult to separate from silicon carbide. Solving the linear system of (24) and (25), we find the initial conditions

$$S^0_{\mathrm{SiO_2}} = \frac{1-\phi_0}{1 + 3\dfrac{\rho_{\mathrm{SiO_2}} M_{\mathrm{C}}}{M_{\mathrm{SiO_2}} \rho_{\mathrm{C}}}}, \quad S^0_{\mathrm{C}} = \frac{1-\phi_0}{1 + \dfrac{M_{\mathrm{SiO_2}} \rho_{\mathrm{C}}}{3\rho_{\mathrm{SiO_2}} M_{\mathrm{C}}}}. \tag{26}$$

In a similar manner to the solid system, we view the two conservation laws (8) and (9) and the constant pressure constraint (11) as equations for the gas system variables $G_{\mathrm{SiO}}$, $G_{\mathrm{CO}}$, and $F$. It appears that two boundary (and initial) conditions are required for this system, perhaps for $G_{\mathrm{SiO}}$ and $G_{\mathrm{CO}}$. In fact, this is not the case: we only require a single initial/boundary condition. To see this, we sum the gas conservation laws and, making use of the ideal gas law (11), we obtain an algebraic expression for $F$, given in terms of (derivatives of) the temperature $T$ and bed cross-sectional area $A$, namely

$$F = T\left(2\frac{AR}{P_a} r_1 - \phi_0 \frac{\partial}{\partial t}\left(\frac{A}{T}\right) - \phi_0 \frac{\partial}{\partial x}\left(\frac{Au}{T}\right)\right). \tag{27}$$

The ideal gas law (11) and one of the conservation laws, (8) or (9), then fix the gas concentrations. Since the concentration of silicon monoxide impacts the reaction kinetics, we keep (8) for $G_{\mathrm{SiO}}$, and view (11) as an equation for $G_{\mathrm{CO}}$. Thus we only require a boundary (and initial) condition for $G_{\mathrm{SiO}}$. Physically, since we specify atmospheric pressure, the temperature sets the amount of gas that can exist in the bed via the ideal gas law. The flux of gas out of the bed $F$ is whatever is produced by the reactions that cannot remain within the bed, since we allow no build up of gas pressure in the bed. The composition of the gas within the bed, i.e., the fraction that is silicon monoxide and that is carbon monoxide, is determined by the relative reaction rates, via the (single) conservation law (8). In reality, at the kiln inlet the gas in the bed is likely to be mostly air, which we do not include in the model since the silicon monoxide and carbon monoxide are produced at such large quantities in the hot zone of the kiln that we can neglect any air near the inlet. To easily quantify the amount silicon lost in the

silicon monoxide gas, we make the artificial assumption that, at the inlet, the gas in the bed is purely carbon monoxide, so that we introduce no additional silicon in the gas this way. Thus we will set

$$G_{\mathrm{SiO}} = 0 \quad \text{at } x = 0 \text{ (and at } t = 0). \tag{28}$$

The physical interpretation of this useful modelling device is that the gas in the cold bed entering the furnace is purely carbon monoxide (rather than air, as is true in reality). Since the carbon monoxide is not a reactant in either of our reaction (1) or (2), it does not affect any of the subsequent reactions.

Finally, we must also impose a boundary (and initial) condition for $n_{\mathrm{C}}$ and $T$, so that the conservation laws (7) and (13) are well-posed. We prescribe an initial radius of carbon particles $r_{\mathrm{C}}^0$, and so we write the inlet number density of carbon as

$$n_{\mathrm{C}}^0 = \frac{S_{\mathrm{C}}^0}{4/3\pi (r_{\mathrm{C}}^0)^3} \quad \text{at } x = 0 \text{ (and at } t = 0), \tag{29}$$

where we have assumed the carbon particles are spherical and that the volume scales as $4/3\pi (r_{\mathrm{C}}^0)^3$. The inlet temperature is

$$T = T_0 \quad \text{at } x = 0 \text{ (and at } t = 0), \tag{30}$$

which we expect to be roughly room temperature, significantly lower than the hot temperatures attained in the hot zone of the kiln.

In summary, following the re-formulation in this section, the model consists of the six conservation laws (4), (5), (7), (8), (13), and (22), with the corresponding six boundary and initial conditions (23), (28) (29), and (30), along with the five algebraic constraints (10), (11), (14), (15), and (27), and the reaction kinetics (16) and (20). This is a closed system for the eleven variables in (21).

Our model contains many dimensional parameters. Typical values for our dimensional parameters are given in Table 1. The uncertainty of the value of each parameter varies largely from parameter to parameter. Physical constants, such as the density of carbon or the molar mass of silicon carbide, are accurately known. However, the rate constants must be estimated from related experiments.

## 3 Nondimensionalisation of the bed problem

We now nondimensionalise the problem within the bed using scalings that are either imposed externally or are inherent to the equations. We first define the scalings we will use for the nondimensionalisation, then we present the dimensionless system, before discussing the interpretation of the dimensionless parameters and their values.

**Table 1** Assumed values of physical parameters in the model

| Parameter | Description | Value | Units | Ref. |
|---|---|---|---|---|
| *Molar masses* | | | | |
| $M_{SiO_2}$ | Molar mass of quartz | $60 \times 10^{-3}$ | kg / mol | [39] |
| $M_C$ | Molar mass of carbon | $12 \times 10^{-3}$ | kg / mol | [39] |
| $M_{SiC}$ | Molar mass of silicon carbide | $40 \times 10^{-3}$ | kg / mol | [39] |
| $M_{SiO}$ | Molar mass of silicon monoxide | $44 \times 10^{-3}$ | kg / mol | [39] |
| $M_{CO}$ | Molar mass of carbon monoxide | $28 \times 10^{-3}$ | kg / mol | [39] |
| *Bulk densities* | | | | |
| $\rho_{SiO_2}$ | Density of quartz | $2.65 \times 10^3$ | kg / m$^3$ | |
| $\rho_C$ | Density of carbon | $2.27 \times 10^3$ | kg / m$^3$ | |
| $\rho_{SiC}$ | Density of silicon carbide | $3.21 \times 10^3$ | kg / m$^3$ | |
| *Specific heats* | | | | |
| $c_{SiO_2}$ | Specific heat of quartz | 1316 | J / kg K | [40] |
| $c_C$ | Specific heat of carbon | 2091 | J / kg K | [40] |
| $c_{SiC}$ | Specific heat of silicon carbide | 1345 | J / kg K | [40] |
| $c_{SiO}$ | Specific heat of silicon monoxide | 848 | J / kg K | [40] |
| $c_{CO}$ | Specific heat of carbon monoxide | 1294 | J / kg K | [40] |
| *Heat capacity* | | | | |
| $\rho_S c_S$ | Volumetric heat capacity of the solid | $2.56 \times 10^6$ | J / m$^3$ K | (44) |

**Table 1** continued

| Parameter | Description | Value | Units | Ref. |
|---|---|---|---|---|
| *Heats of reaction* | | | | |
| $\Delta H_1$ | Enthalpy of reaction (1) | $792 \times 10^3$ | J / mol($SiO_2$) | [41] |
| $\Delta H_2$ | Enthalpy of reaction (2) | $-78 \times 10^3$ | J / mol(SiO) | [41] |
| *Geometric / flow parameters* | | | | |
| $L$ | Length of reactor | 30 | m | |
| $Q_0$ | External heating | $10^6$ | J / m s | |
| $A_0$ | Initial cross-sectional area of solid | 1 | $m^2$ | |
| $\phi_0$ | Porosity | 0.36 | - | [42] |
| $r_C^0$ | Initial carbon particle radius | $10^{-5}$ | m | |
| *Kinetic / thermodynamic constants* | | | | |
| $k_1$ | Reaction (1) rate constant | $10^8$ | mol($SiO_2$) / $m^3$ s | |
| $k_2$ | Reaction (2) rate constant | $10^{-4}$ | m / s | |
| $E_1$ | Reaction (1) activation energy | $3.3 \times 10^5$ | J / mol | [18] |
| $R$ | Universal gas constant | 8.314 | J / mol K | |
| $P_a$ | Ambient pressure | $10^5$ | Pa | |
| *Inlet conditions* | | | | |
| $A_0$ | Cross-sectional area | 1 | $m^2$ | |
| $S^0_{SiO_2}$ | Volume fraction of quartz | 0.3767 | - | |
| $S^0_C$ | Volume fraction of carbon | 0.2633 | - | |
| $T_0$ | Temperature | 300 | K | |

**Table 2** Intrinsic scalings computed from the values in Table 1

| Variable | Value | Unit |
|---|---|---|
| $u^*$ | $8.58 \times 10^{-4}$ | m / s |
| $G^*_{\mathrm{SiO}}$ | 0.318 | mol / m$^3$ |
| $G^*_{\mathrm{CO}}$ | 5.51 | mol / m$^3$ |
| $T^*$ | 2182.4 | K |
| $F^*$ | 0.230 | m$^2$ / s |

### 3.1 Scalings

We adopt the natural scalings

$$x = L\hat{x}, \quad t = \frac{L}{u^*}\hat{t}, \quad A = A_0\hat{A}, \quad n_{\mathrm{C}} = \frac{S^0_{\mathrm{C}}}{\frac{4}{3}\pi(r^0_{\mathrm{C}})^3}\hat{n}_{\mathrm{C}}, \tag{31}$$

where $\hat{\cdot}$ denotes a dimensionless quantity, $L$ is the length of the kiln, $u^*$ is the intrinsic velocity of the solid material through the kiln (defined in (34) below), $L/u^*$ is the velocity timescale, and $A_0$ and $\frac{S^0_{\mathrm{C}}}{4/3\pi(r^0_{\mathrm{C}})^3}$ are the inlet cross-sectional area of the solid material and number density at the inlet of the kiln, respectively. We choose to scale the solid velocity, gas concentrations, temperature, and the gas flux out of the bed by

$$u = u^*\hat{u}, \quad G_{\mathrm{SiO}} = G^*_{\mathrm{SiO}}\hat{G}_{\mathrm{SiO}}, \quad G_{\mathrm{CO}} = G^*_{\mathrm{CO}}\hat{G}_{\mathrm{CO}}, \tag{32}$$

$$T = T^*\left(1 + \frac{RT^*}{E_1}\hat{T}\right), \quad F = F^*\hat{F}, \tag{33}$$

where we have introduced the intrinsic scalings

$$u^* = \frac{Q_0 L M_{\mathrm{SiO_2}}}{A_0 \Delta H_1 \rho_{\mathrm{SiO_2}}}, \quad G^*_{\mathrm{SiO}} = \frac{\left(\frac{4}{3}\pi\right)^{1/3} Q_0 r^0_{\mathrm{C}}}{A_0 \Delta H_1 k_2 (S^0_{\mathrm{C}})^{1/3}}, \quad G^*_{\mathrm{CO}} = \frac{P_a}{RT*}, \tag{34}$$

$$T^* = -\frac{E_1}{R\log\left(\frac{Q_0}{A_0\Delta H_1 k_1}\right)}, \quad F^* = \frac{Q_0}{G^*_{\mathrm{CO}}\Delta H_1}. \tag{35}$$

The intrinsic velocity $u^*$ is chosen to balance the solid velocity with reaction (1). The scaling $G^*_{\mathrm{SiO}}$ is chosen so that the two reaction rates balance, $G^*_{\mathrm{CO}}$ is chosen so that $\hat{G}_{\mathrm{CO}} = 1$ at the hot-zone temperature of $\hat{T} = 0$ (in the absence of silicon monoxide). The temperature scale $T^*$ is the intrinsic temperature of the system based on the balance of the applied heating and enthalpy of reaction (1). We expect the temperature to be close to this value in the hot zone of the kiln. Finally, the intrinsic scaling of the gas flux $F^*$ is the ratio of the energy supplied to the energy consumed by reaction (1).

We note that our choice of $T^*$ gives the convenient relation

$$k_1 \exp\left(-\frac{E_1}{RT^*}\right) = \frac{Q_0}{A_0 \Delta H_1}. \tag{36}$$

We estimate the values of the intrinsic scalings in Table 2 using the values given in Table 1. Initially, the intrinsic velocity $u^*$ may appear quite slow; however, it corresponds to a speed of approximately 3 m / hr, which is typical for rotary kilns. The intrinsic concentration scale of silicon monoxide is found to be about an order of magnitude smaller than that of carbon monoxide. This is consistent with expectations: the carbon monoxide scale is derived from the ideal gas law, while silicon monoxide is rapidly consumed by reaction (2), resulting in a lower characteristic concentration. The intrinsic temperature $T^*$ is approximately 150 K higher than the ideal operating temperature for silicon carbide production. However, this difference is not concerning, as our values for the supplied heating rate $Q_0$ and the reaction rate constant $k_1$ are only rough, order-of-magnitude estimates. With improved experimental data for $k_1$, we could hone $Q_0$ to bring $T^*$ closer to the desired range. Finally, the estimated value of $F^*$, which represents the volumetric flux of gas through the top of the bed, appears physically reasonable. Given that the exposed bed width is on the order of the kiln diameter and that typical gas velocities in this region are modest, the resulting flux is expected to be relatively small. Our estimate aligns with this expectation.

### 3.2 Dimensionless equations

After using the scalings previously outlined, and dropping the hat notation, the dimensionless versions of the model for the solid volume fractions of quartz and carbon (4) and (5), the no voids condition (10), and number density (7), read

$$\frac{\partial}{\partial t}\left(AS_{\mathrm{SiO_2}}\right) + \frac{\partial}{\partial x}\left(AS_{\mathrm{SiO_2}}u\right) = -Ar_1, \tag{37}$$

$$\frac{\partial}{\partial t}\left(AS_{\mathrm{C}}\right) + \frac{\partial}{\partial x}\left(AS_{\mathrm{C}}u\right) = -\mathcal{C}_{\mathrm{C}}A(r_1 + 2r_2), \tag{38}$$

$$S_{\mathrm{SiO_2}} + S_{\mathrm{C}} + S_{\mathrm{SiC}} = 1 - \phi_0, \tag{39}$$

$$\frac{\partial}{\partial t}\left(An_{\mathrm{C}}\right) + \frac{\partial}{\partial x}\left(An_{\mathrm{C}}u\right) = 0, \tag{40}$$

while the cross-sectional area equation (22) reads

$$(1-\phi_0)\left(\frac{\partial A}{\partial t} + \frac{\partial}{\partial x}(Au)\right) = A\Big(-(1+\mathcal{C}_{\mathrm{C}})r_1 + (\mathcal{C}_{\mathrm{SiC}} - 2\mathcal{C}_{\mathrm{C}})r_2\Big). \tag{41}$$

The silicon monoxide concentration equation (8) becomes

$$\delta\left(\frac{\partial}{\partial t}\left(AG_{\mathrm{SiO}}\right) + \frac{\partial}{\partial x}\left(AG_{\mathrm{SiO}}u\right)\right) + FG_{\mathrm{SiO}} = \Gamma A(r_1 - r_2), \tag{42}$$

and the dimensionless version of the temperature equation (13) is

$$\tau\left(\frac{\partial}{\partial t}\left(A(1+\epsilon T)\right)+\frac{\partial}{\partial x}\left(A(1+\epsilon T)u\right)\right) + \sigma\left(G_{\mathrm{CO}}+\frac{\mathcal{M}}{\Gamma}G_{\mathrm{SiO}}\right)(1+\epsilon T)F = Q - Ar_1 + \mathcal{H}Ar_2. \tag{43}$$

We note here that we have made one further assumption, namely that the volumetric heat capacity $\rho_S c_S$ is constant and independent of solid composition. The methods presented can accommodate the more general case, but at the expense of much more complicated algebra, which we wish to avoid to prioritise insight. We will see that the transport terms in (43) are only part of the dominant balance in the pre-heat zone, where the solids are brought up to reaction temperature. We thus approximate the volumetric heat capacity as

$$\rho_S c_S = S^0_{\mathrm{SiO_2}}\rho_{\mathrm{SiO_2}}c_{\mathrm{SiO_2}} + S^0_{\mathrm{C}}\rho_{\mathrm{C}}c_{\mathrm{C}}. \tag{44}$$

The gas concentrations and temperature are also related by the ideal gas law (11), which reads

$$\left(\frac{1}{\Gamma}G_{\mathrm{SiO}}+G_{\mathrm{CO}}\right)(1+\epsilon T) = 1. \tag{45}$$

The equation (27) for $F$ becomes

$$F = (1+\epsilon T)\left(2Ar_1 - \delta\left(\frac{\partial}{\partial t}\left(\frac{A}{1+\epsilon T}\right)-\frac{\partial}{\partial x}\left(\frac{Au}{1+\epsilon T}\right)\right)\right). \tag{46}$$

Lastly, the dimensionless flow equation (15) is

$$f(u, A; \omega, \alpha, \dots) = 0. \tag{47}$$

The reaction kinetics given by (16) and (20) become

$$r_1 = \exp\left(\frac{T}{1+\epsilon T}\right)S_{\mathrm{SiO_2}}S_{\mathrm{C}}, \quad r_2 = \left(n_{\mathrm{C}}S_{\mathrm{C}}^2\right)^{1/3}\phi_0 G_{\mathrm{SiO}}, \tag{48}$$

in dimensionless form.

The dimensionless versions of the boundary and initial conditions (23), (26), and (28)–(30) become

$$S_{\mathrm{SiO_2}} = 0.3767, \quad S_{\mathrm{C}} = 0.2633, \quad n_{\mathrm{C}} = 1, \tag{49}$$

$$A = 1, \quad G_{\mathrm{SiO}} = 0, \quad T = \frac{\mathcal{T}-1}{\epsilon}. \tag{50}$$

**Table 3** Dimensionless parameter values, given by (51), computed from the values in Table 1

| Parameter | Description | Value |
|---|---|---|
| $\mathcal{C}_{\mathrm{C}}$ | Concentration ratio of quartz to carbon | 0.233 |
| $\mathcal{C}_{\mathrm{SiC}}$ | Concentration ratio of quartz to silicon carbide | 0.550 |
| $\delta$ | Gas to solid concentration ratio | $4.49 \times 10^{-5}$ |
| $\Gamma$ | Intrinsic gas concentration ratio | 17.33 |
| $\tau$ | Length of pre-heat zone | 0.102 |
| $\sigma$ | Thermal energy transported out of the bed to enthalpy ratio | 0.100 |
| $\mathcal{M}$ | Molar heat capacity ratio | 1.030 |
| $\mathcal{H}$ | Enthalpies of reaction ratio | 0.098 |
| $\epsilon$ | Gas energy to activation energy ratio | 0.0550 |
| $\mathcal{T}$ | Inlet temperature to intrinsic temperature ratio | 0.137 |

### 3.3 Dimensionless parameter groups

The 10 dimensionless numbers we have introduced into the problem are

$$\begin{gathered}\mathcal{C}_{\mathrm{C}} = \frac{M_{\mathrm{C}}}{\rho_{\mathrm{C}}}\frac{\rho_{\mathrm{SiO_2}}}{M_{\mathrm{SiO_2}}}, \quad \mathcal{C}_{\mathrm{SiC}} = \frac{M_{\mathrm{SiC}}}{\rho_{\mathrm{SiC}}}\frac{\rho_{\mathrm{SiO_2}}}{M_{\mathrm{SiO_2}}}, \quad \delta = \frac{\phi_0 M_{\mathrm{SiO_2}} G^*_{\mathrm{CO}}}{\rho_{\mathrm{SiO_2}}} = \frac{\phi_0 P_a M_{\mathrm{SiO_2}}}{RT^* \rho_{\mathrm{SiO_2}}}, \\ \Gamma = \frac{G^*_{\mathrm{CO}}}{G^*_{\mathrm{SiO}}} = \frac{P_a A_0 \Delta H_1 k_2 (S^0_{\mathrm{C}})^{1/3}}{\left(\frac{4}{3}\pi\right)^{1/3} RT^* Q_0 r^0_{\mathrm{C}}}, \quad \tau = \frac{(1-\phi_0) M_{\mathrm{SiO_2}} \rho_S c_S T^*}{\Delta H_1 \rho_{\mathrm{SiO_2}}}, \\ \sigma = \frac{M_{\mathrm{CO}} c_{\mathrm{CO}} T^*}{\Delta H_1}, \quad \mathcal{M} = \frac{M_{\mathrm{SiO}} c_{\mathrm{SiO}}}{M_{\mathrm{CO}} c_{\mathrm{CO}}}, \quad \mathcal{H} = \left|\frac{\Delta H_2}{\Delta H_1}\right|, \quad \epsilon = \frac{RT^*}{E_1}, \quad \mathcal{T} = \frac{T_0}{T^*}.\end{gathered} \tag{51}$$

The $\mathcal{C}_{\mathrm{C}}$ and $\mathcal{C}_{\mathrm{SiC}}$ are the 'concentration' ratios of quartz to carbon and silicon carbide, respectively. The concentration ratio of gas to quartz is denoted by $\delta$. The parameter $\Gamma$ is the ratio of the intrinsic concentration scales of carbon monoxide to silicon monoxide. The parameter $\tau$ is the ratio of the thermal energy of the solid to the energy consumed by reaction (1). Alternatively, as we will see in Sect. 4, $\tau$ can be viewed as the length of the pre-heating zone, over which the solid materials are heated from the initial temperature to the intrinsic temperature. Similarly, $\sigma$ is the ratio of thermal energy transported out of the bed by the gas to the energy of reaction (1). The parameter $\mathcal{M}$ is the ratio of the molar heat capacities of silicon monoxide and carbon dioxide. The (absolute) ratio of the enthalpies of reaction (2) to reaction (1) is denoted by $\mathcal{H}$. The ratio of the energy of the system to the activation energy of reaction (1) is encapsulated by $\epsilon$. Finally, $\mathcal{T}$ is the ratio of the temperature at the inlet to the intrinsic temperature of the system.

Values of these dimensionless parameters are given in Table 3, which we compute from the values of dimensional parameters given in Table 1. We note that our ability to control or vary the values of these dimensionless parameters experimentally varies from parameter to parameter. The parameters $\mathcal{C}_{\mathrm{C}}$, $\mathcal{C}_{\mathrm{SiC}}$, $\mathcal{M}$, and $\mathcal{H}$ are defined by known physical parameters, and thus, cannot be altered by modifying an experimental set-up.

Similarly, the only dimensional parameter within $\delta$, $\tau$, $\sigma$, $\epsilon$, and $\mathcal{T}$ that we have any control over is $T^*$, which in turn is controlled by the value of $Q_0/A_0k_1$. However, we have a fairly narrow range of operating temperatures in order to have the correct chemical reactions be dominant. The only dimensionless parameter remaining is $\Gamma$. Notice that we may rewrite

$$\Gamma = \frac{P_a(S_c^0)^{1/3}k_2}{\left(\frac{4}{3}\pi\right)^{1/3} RT^*k_1r_c^0} \exp\left(\frac{E_1}{RT^*}\right), \tag{52}$$

using (36). In this form, it is clear that $\Gamma$ depends only on accurately known physical parameters, $T^*$, and the grouping $k_2/k_1r_c^0$. Therefore, the dynamics of the system only depend on the dimensional groupings $Q_0/A_0k_1$ (to define $T^*$) and $k_2/k_1r_c^0$ (to define $\Gamma$). Here, the rate constants $k_1$ and $k_2$ are also physical parameters with values that we cannot modify. However, in practice it is difficult to measure the value of these parameters. We are unlikely to have a very accurate estimate of their values, and so we include them in these groupings. We investigate the effect of these dimensionless groupings on the kiln performance in the following sections.

## 4 Asymptotic analysis of the steady-state problem

One major benefit of rotary kilns is that they may be operated continuously, unlike batch kilns. Therefore, while the start-up dynamics may play an important role in pilot- or laboratory-experiments, we are primarily concerned with the steady-state operation. With this in mind, in this section we analyse the steady-state system, noting the different spatial regions where the dominant balances shift, to develop intuition for the expected behaviour within the kiln. To facilitate the investigation, we impose two further simplifying assumptions on the steady-state model:

1. **Quasi-static gas:** We assume $\delta \ll 1$. Recall that $\delta$ is related to the ratio of the concentration of the gas to the concentration of the solid. This parameter is much smaller than the rest (see Table 3), and will always be negligible for any experimental set-up of practical use.
2. **Constant solid velocity:** In order to proceed with the analysis we require a form of $f$ for the solid flow in (47). Motivated by the need for a simple preliminary model, we are guided by the discussions in [24, 43], who indicate it is reasonable to assume that

$$u \propto \frac{D\,\omega\,\alpha}{\sqrt{\varphi_{\text{bed}}}}, \tag{53}$$

where $D$ is the kiln diameter, $\omega$ is the kiln rotation speed, $\alpha$ the inclination of the kiln, and $\varphi_{\text{bed}}$ is the angle of repose. Hence, for the model here we take $u$ as constant.

Our quasi-static assumption that $\delta \ll 1$ changes the structure of the system by removing the transport terms from the gas concentration equations (42) and (46). The concentration of the gas is much less than the concentration of the solid, and so

the gas responds much quicker than the solid. A consequence is that we no longer require boundary or initial conditions for concentration of silicon monoxide in (42).

With these assumptions, our dimensionless model (42)–(48) reduces to

$$u\frac{\mathrm{d}}{\mathrm{d}x}\left(AS_{\mathrm{SiO_2}}\right) = -Ar_1, \tag{54}$$

$$u\frac{\mathrm{d}}{\mathrm{d}x}\left(AS_{\mathrm{c}}\right) = -\mathcal{C}_{\mathrm{c}}A(r_1 + 2r_2), \tag{55}$$

$$S_{\mathrm{SiO_2}} + S_{\mathrm{c}} + S_{\mathrm{SiC}} = 1 - \phi_0, \tag{56}$$

$$u\frac{\mathrm{d}}{\mathrm{d}x}\left(An_{\mathrm{c}}\right) = 0, \tag{57}$$

$$(1-\phi_0)u\frac{\mathrm{d}A}{\mathrm{d}x} = A\Big( -(1+\mathcal{C}_{\mathrm{c}})r_1 + (\mathcal{C}_{\mathrm{SiC}} - 2\,\mathcal{C}_{\mathrm{c}})r_2\Big), \tag{58}$$

$$FG_{\mathrm{SiO}} = \Gamma A(r_1 - r_2), \tag{59}$$

$$F = 2Ar_1(1+\epsilon T), \tag{60}$$

$$\tau u\frac{\mathrm{d}}{\mathrm{d}x}\left(A(1+\epsilon T)\right) + \sigma\left(G_{\mathrm{CO}} + \frac{\mathcal{M}}{\Gamma}G_{\mathrm{SiO}}\right)(1+\epsilon T)F = Q - Ar_1 + \mathcal{H}Ar_2, \tag{61}$$

$$\left(\frac{1}{\Gamma}G_{\mathrm{SiO}} + G_{\mathrm{CO}}\right)(1+\epsilon T) = 1, \tag{62}$$

$$u = \text{constant}. \tag{63}$$

Our assumption that $u$ is constant means that this steady-state problem behaves like a standard lumped chemical-reaction system of ODEs: the spatial variable $x$ behaves as the time-like variable as we follow the material through the reactor.

Moreover, we can now eliminate $n_{\mathrm{c}}$ from the system in the following way. We can integrate the simple form of (57) to find that

$$An_{\mathrm{c}} = 1, \quad \text{i.e.} \quad n_{\mathrm{c}} = \frac{1}{A}, \tag{64}$$

by applying the boundary conditions (49) and (50). We may now substitute this into the reaction rate so that

$$r_2 = \phi_0\left(\frac{S_{\mathrm{c}}^2}{A}\right)^{1/3} G_{\mathrm{SiO}}, \tag{65}$$

and now $n_{\mathrm{c}}$ no longer appears in the system. We also note that the axial reaction rate of reaction (2) (as it appears in all our equations) is $Ar_2 = \phi_0(AS_{\mathrm{c}})^{2/3}G_{\mathrm{SiO}}$. This axial reaction rate is proportional to the total surface area of carbon particles, $(AS_{\mathrm{c}})^{2/3}$, as we might expect for a surface-area dependent reaction rate [22, 44].

The steady-state model now consists of four conservation laws (54), (55), (58) and (61), which require four boundary conditions. We impose $A = 1$, $S_{\mathrm{SiO_2}} = S^0_{\mathrm{SiO_2}}$,

$S_c = S_c^0$, and $T = (\mathcal{T} - 1)/\epsilon$ from (49) and (50). These are supplemented by five algebraic constraints (56), (59), (60), (62) and (63), along with the reaction rates $r_1$ and $r_2$, given by (48) and (65), to fully define the system.

As introduced in [21, 44], we now define two metrics to help characterise the system dynamics. The first is the *silicon carbide yield*, defined as

$$Y_{\text{SiC}}(x) = \frac{A(x)S_{\text{SiC}}(x)}{\mathcal{C}_{\text{SiC}}S_{\text{SiO}_2}^0}, \tag{66}$$

which represents the molar flux of silicon carbide, normalised by the molar flux of quartz at the inlet. A yield of $Y_{\text{SiC}} = 1$ indicates complete conversion of the silicon atoms originally present in the supplied quartz to silicon carbide. Maximising silicon yield is the primary operational goal for Elkem ASA. We are most interested in the silicon carbide yield at the outlet at $x = 1$.

The second metric is the *carbon utilisation*, defined as

$$U_{\text{C}}(x) = 1 - \frac{A(x)S_{\text{C}}(x)}{S_{\text{C}}^0}, \tag{67}$$

which quantifies the fraction of the initial carbon that is consumed by the chemical reactions. A secondary objective for Elkem ASA is to minimise the excess carbon extracted from the kiln (and therefore maximise $U_{\text{C}}$). In more chemically complex systems, the carbon utilisation can serve as a proxy for comparing relative reaction speeds, such as in [21, 22, 44]. However, in the context of the simplified reaction scheme considered here, we expect the two metrics to be strongly correlated, as there is only one reaction pathway. Carbon and quartz are consumed at the same rate in reaction (1), and carbon is consumed at twice the rate that silicon carbide is produced in reaction (2). Indeed, in our chemical system

$$U_{\text{C}} = \frac{1}{3}\left(2Y_{\text{SiC}} + 1 - \frac{AS_{\text{SiO}_2}}{S_{\text{SiO}_2}^0}\right), \tag{68}$$

so that maximising silicon carbide yield is equivalent to maximising carbon utilisation by (68). Within our analysis we will focus on the silicon carbide yield, but still report the carbon utilisation as it is a valuable metric.

Finally, we note that an alternative way to think about the loss of silicon from the bed is to consider the residence time of the SiO gas within the bed: a larger residence time is likely to result in higher silicon re-capture, via reaction (2). The gas mixture escapes the bed at rate $F$ [$\text{m}^2\text{s}^{-1}$]; this is the volumetric gas loss [$\text{m}^3\text{s}^{-1}$] per unit along-kiln length [m]. We can use this to estimate both the velocity of the gas and the residence time: if the interface between the bed and channel has length $l$ (interfacial area per unit along-kiln length) then the gas velocity coming out of the bed is estimated as $F/l$ [$\text{m}\,\text{s}^{-1}$]. If $d$ is the height of the bed, the residence time is estimated as $d/(F/l) = dl/F = A/F$ [s] (since $A \sim dl$). Using the scales for $F_*$ and $A_0$ in Tables 1 and 2, we therefore estimate a residence time on the order of 4 s.

### 4.1 Asymptotic structure

Some helpful insight concerning the general behaviour of the solution of the problem can be found by considering a relevant asymptotic limit of the parameters. In this section we assume that the parameters $\tau \ll 1, \sigma \ll 1, \mathcal{H} \ll 1, \epsilon \ll 1, \mathcal{T} = \mathcal{O}(\epsilon)$, and all other parameters to be $\mathcal{O}(1)$. Physically, this regime has the following interpretations. Solids are brought from their initial temperature up to reaction temperature over a short length compared to the length of the kiln ($\tau \ll 1$). Only a small fraction of energy is lost due to the gas flow out of the bed ($\sigma \ll 1$). The enthalpy change associated with reaction (2) is small relative to that of reaction (1) ($\mathcal{H} \ll 1$). The thermal energy in the bed is small compared to the activation energy reaction (1) ($\epsilon \ll 1$). The inlet feed temperature is low compared to the intrinsic temperature ($\mathcal{T} = \mathcal{O}(\epsilon)$).

Although various special cases arise depending on the relative size of the small parameters, here we consider the general structure of the solution. The resulting problem has three crucial zones, the pre-heat zone, the hot zone and the post-reaction zone. The transitions between these regimes occur over very short lengthscales of $\mathcal{O}(\epsilon\tau)$, forming thin layers that smooth the transition between zones. The dynamics within these layers are explored in detail in Appendix A. This structure is reminiscent of the asymptotic structures found in [34] for traditional submerged-arc silicon furnaces, despite the different heat source for the reactions in that case.

As we will show in this section, the zones arise due to changes in the dominant physical balances, particularly in the temperature equation (61). In the pre-heat zone, located near the inlet, the temperature of the solid materials steadily increases, but remains below the threshold for reaction, so no gas is produced. As the temperature increases further, and approaches the onset temperature for reaction, we enter a narrow pre-heat transition zone where reactions begin and gas production is initialised. Beyond the pre-heat transition zone is the hot zone, where the majority of the chemical reactions take place. In the hot zone, the temperature remains close to its intrinsic value, and reactions proceed rapidly, such that most of the gas and silicon carbide is produced in this zone. Once most of the quartz has been consumed, reaction (1) slows, and gas production is significantly reduced in a second narrow transition layer. Finally, once all of the quartz has been consumed, we enter the post-reaction zone. In this region, reactions cease, and the system reverts to a similar balance as in the pre-heat zone: heating is balanced by advection, and the temperature in the bed rises dramatically without further reactions occurring.

This basic structure, summarised in Fig. 2, seems to be inherent to any practical kiln that might react a substantial fraction of the quartz, and hence seems a good starting point for understanding the behaviour in the kiln.

### 4.2 Pre-heat zone

In the pre-heat zone, since $\mathcal{T} \ll 1$, the boundary condition (50) implies that the temperature is very large (and negative) so we find that $T = \mathcal{O}(1/\epsilon)$, while the gas concentrations remain $\mathcal{O}(1)$ or very small. The large, negative temperature suppresses the Arrhenius reaction rate $r_1$, which is exponentially small. Therefore, the silicon

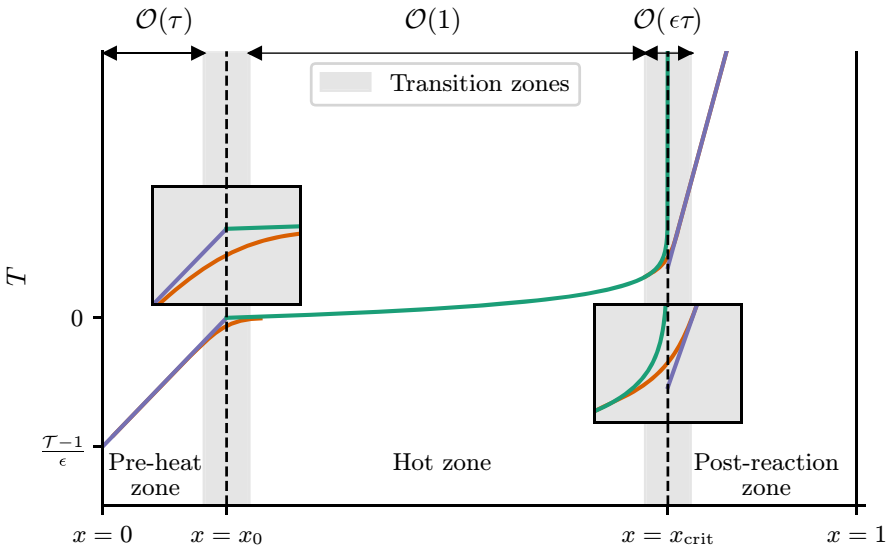


**Fig. 2** Schematic of the steady-state solution structure. Distinct dominant balances in the temperature equation (61) give rise to three zones (pre-heat, hot, and post-reaction). These zones are separated by two narrow transition zones of $\mathcal{O}(\epsilon\tau)$, located about $x_0$ and $x_{\text{crit}}$. Here we use a uniform applied heat flux $Q$, but the structure is the same for a spatially varying $Q$ so long as it remains $\mathcal{O}(1)$ everywhere

monoxide concentration, and thus $r_2$, are negligible. Consequently, the concentration of carbon monoxide is $G_{\text{CO}} = 1/(1+\epsilon T)$, which remains $\mathcal{O}(1)$. The only non-trivial dynamics result from the dominant balance between the advective sensible heat and the external heating $Q$ in the temperature equation (61). This balance implies that the lengthscale of the pre-heat zone is $\mathcal{O}(\tau) \ll 1$.

In the absence of reactions no significant gas flow occurs ($F$ is exponentially small), and the solid volume fractions and the cross-sectional area of the bed remain fixed at their inlet values. The required temperature rise of $\mathcal{O}(1/\epsilon)$ from the boundary condition (50) occurring over a length scale $\mathcal{O}(\tau)$ leads to a steep temperature gradient of $\mathcal{O}(1/\epsilon\tau)$. Integrating (61) yields the leading-order temperature profile

$$T = \frac{1}{\epsilon}\left(\mathcal{T} - 1 + \frac{1}{\tau u}\int_0^x Q(\bar{x})\,\mathrm{d}\bar{x}\right). \tag{69}$$

The pre-heat region ends as the temperature approaches 0, where the dominant balance in the problem shifts. In the temperature equation (61), the reaction rates become $\mathcal{O}(1)$ and balance the advective sensible heat and the external heating. This transition occurs in a narrow layer of length $\mathcal{O}(\epsilon\tau)$ about the transition point $x_0$. Taking this change in balance to occur at $T \approx 0$ (an assumption that is accurate to leading-order), the transition point $x_0$ is given implicitly by the relationship

$$\int_0^{x_0} Q(\bar{x})\,\mathrm{d}\bar{x} \approx \tau u\,(1-\mathcal{T})\,. \tag{70}$$

In this transition layer the solid volumes and cross-sectional area remain constant, while silicon monoxide production is initialised, but slow. The intricacies of the leading-order dynamics in this zone are clarified in Appendix A.1. Reactions and chemical production begin in earnest in the hot zone, which follows.

### 4.3 Analysis of the hot zone

We recall that in the nondimensionalisation we chose the scales for all variables using balances appropriate for this hot zone, so we expect that all dependent variables are $\mathcal{O}(1)$. To leading-order in the hot zone, the dimensionless model (42)–(48) becomes the much simpler system

$$u\frac{\mathrm{d}}{\mathrm{d}x}\left(AS_{\mathrm{SiO_2}}\right) = -A\mathrm{e}^{T}S_{\mathrm{SiO_2}}S_{\mathrm{C}}, \tag{71}$$

$$u\frac{\mathrm{d}}{\mathrm{d}x}\left(AS_{\mathrm{C}}\right) = -\mathcal{C}_{\mathrm{C}}\left(A\mathrm{e}^{T}S_{\mathrm{SiO_2}}S_{\mathrm{C}} + 2(AS_{\mathrm{C}})^{2/3}\phi_0 G_{\mathrm{SiO}}\right), \tag{72}$$

$$S_{\mathrm{SiO_2}} + S_{\mathrm{C}} + S_{\mathrm{SiC}} = 1 - \phi_0, \tag{73}$$

$$(1-\phi_0)u\frac{\mathrm{d}A}{\mathrm{d}x} = -(1+\mathcal{C}_{\mathrm{C}})A\mathrm{e}^{T}S_{\mathrm{SiO_2}}S_{\mathrm{C}} + (\mathcal{C}_{\mathrm{SiC}} - 2\mathcal{C}_{\mathrm{C}})(AS_{\mathrm{C}})^{2/3}\phi_0 G_{\mathrm{SiO}}, \tag{74}$$

$$FG_{\mathrm{SiO}} = \Gamma\left(A\mathrm{e}^{T}S_{\mathrm{SiO_2}}S_{\mathrm{C}} - (AS_{\mathrm{C}})^{2/3}\phi_0 G_{\mathrm{SiO}}\right), \tag{75}$$

$$F = 2A\mathrm{e}^{T}S_{\mathrm{SiO_2}}S_{\mathrm{C}}, \tag{76}$$

$$0 = Q - A\mathrm{e}^{T}S_{\mathrm{SiO_2}}S_{\mathrm{C}}, \tag{77}$$

$$\frac{1}{\Gamma}G_{\mathrm{SiO}} + G_{\mathrm{CO}} = 1, \tag{78}$$

$$u = \text{constant}. \tag{79}$$

From (77), we note that $Q = A\mathrm{e}^{T}S_{\mathrm{SiO_2}}S_{\mathrm{C}}$, so that the rate of reaction (1) is equal to the prescribed heating rate $Q$. Rearranging, we find that

$$T = \log\left(\frac{Q}{AS_{\mathrm{SiO_2}}S_{\mathrm{C}}}\right). \tag{80}$$

Thus the temperature in the hot zone is set by the balance of heating and endothermic reaction. We note that, each of $S_{\mathrm{SiO_2}}$ and $AS_{\mathrm{C}}$ will decrease through the hot zone, thus $T$ must increase with $x$. The temperature must rise in order that reaction (1) continues at the same rate when there are less reactants available.

Immediately from the gas flow equation (76), using the fact that $Q = A\mathrm{e}^{T}S_{\mathrm{SiO_2}}S_{\mathrm{C}}$, we find

$$F = 2Q, \tag{81}$$

since the heating rate directly sets the gas production rate. Substituting (77) and (81) into (75) we find that

$$G_{\mathrm{SiO}} = \frac{\Gamma Q}{2Q + \phi_0\Gamma(AS_{\mathrm{C}})^{2/3}}, \tag{82}$$

so that, from (78), we obtain

$$G_{\mathrm{CO}} = \frac{Q + \phi_0 \Gamma (A S_{\mathrm{C}})^{2/3}}{2Q + \phi_0 \Gamma (A S_{\mathrm{C}})^{2/3}}. \tag{83}$$

Equation (71) for the volume fraction of quartz is straightforwardly integrated to obtain $S_{\mathrm{SiO_2}}$ in terms of $A$,

$$S_{\mathrm{SiO_2}} = \frac{1}{A}\left(S^0_{\mathrm{SiO_2}} - \frac{1}{u}\int_{x_0}^{x} Q(\bar{x})\,\mathrm{d}\bar{x}\right), \tag{84}$$

where $S^0_{\mathrm{SiO_2}}$ is the prescribed inlet volume fraction of quartz, which from the discussion earlier in this section, is the same at the start of the hot zone, $x = x_0$, as at the inlet of the kiln. From (73), we may also write

$$S_{\mathrm{SiC}} = 1 - \phi_0 - S_{\mathrm{C}} - \frac{1}{A}\left(S^0_{\mathrm{SiO_2}} - \frac{1}{u}\int_{x_0}^{x} Q(\bar{x})\,\mathrm{d}\bar{x}\right). \tag{85}$$

The two remaining ODEs are (72) and (74), which, using our expression for $T$ and for $G_{\mathrm{SiO}}$, may now be written as

$$u\frac{\mathrm{d}}{\mathrm{d}x}(A S_{\mathrm{C}}) = -\mathcal{C}_{\mathrm{C}} Q\left(1 + \frac{2\phi_0 \Gamma (A S_{\mathrm{C}})^{2/3}}{2Q + \phi_0 \Gamma (A S_{\mathrm{C}})^{2/3}}\right), \tag{86}$$

$$u(1-\phi_0)\frac{\mathrm{d}A}{\mathrm{d}x} = -(1+\mathcal{C}_{\mathrm{C}})Q + (\mathcal{C}_{\mathrm{SiC}} - 2\mathcal{C}_{\mathrm{C}})\frac{Q\phi_0 \Gamma (A S_{\mathrm{C}})^{2/3}}{2Q + \phi_0 \Gamma (A S_{\mathrm{C}})^{2/3}}, \tag{87}$$

which is a closed system for $A$ and $S_{\mathrm{C}}$. Indeed, (86) may be integrated to find $A S_{\mathrm{C}}$ implicitly, although this is not particularly instructive. Regardless, upon solution of the system (86) and (87), all other variables ($T$, $F$, $S_{\mathrm{SiO_2}}$, $S_{\mathrm{SiC}}$, $G_{\mathrm{SiO}}$, $G_{\mathrm{CO}}$) are given in terms of $A$ and $S_{\mathrm{C}}$ by (80)–(85).

In our leading-order analysis of the hot zone, chemical reactions continue until all of the quartz is consumed. The quartz is exhausted before the carbon volume fraction reaches zero. To see this, we note from (84) that $S_{\mathrm{SiO_2}} = 0$ when $x = x_{\mathrm{crit}}$, which we implicitly define by

$$u S^0_{\mathrm{SiO_2}} = \int_{x_0}^{x_{\mathrm{crit}}} Q(\bar{x})\,\mathrm{d}\bar{x}. \tag{88}$$

While from (86),

$$u\frac{\mathrm{d}}{\mathrm{d}x}(A S_{\mathrm{C}}) = -\mathcal{C}_{\mathrm{C}} Q\left(1 + \frac{2\phi_0 \Gamma (A S_{\mathrm{C}})^{2/3}}{2Q + \phi_0 \Gamma (A S_{\mathrm{C}})^{2/3}}\right) \geq -3\,\mathcal{C}_{\mathrm{C}} Q, \tag{89}$$

so long as $S_{\mathrm{C}} > 0$, with equality in the limit as $\Gamma \to \infty$. Integrating, we see that

$$u(A S_{\mathrm{C}})|_{x=x_{\mathrm{crit}}} \geq u S^0_{\mathrm{C}} - 3\,\mathcal{C}_{\mathrm{C}}\int_{x_0}^{x_{\mathrm{crit}}} Q(\bar{x})\,\mathrm{d}\bar{x} = u\left(S^0_{\mathrm{C}} - 3\,\mathcal{C}_{\mathrm{C}} S^0_{\mathrm{SiO_2}}\right) = 0, \tag{90}$$

using the imposed stoichiometry of the inlet conditions (25), again with equality only in the limit $\Gamma \to \infty$. Thus, the hot zone ends at the point $x = x_{\text{crit}}$ where $S_{\text{SiO}_2} = 0$, while still $S_{\text{C}} > 0$. This is intuitive, since some fraction of the silicon is expected to be lost as silicon monoxide gas, and so some carbon will remain unreacted.

The transition from the hot zone to the post-reaction zone occurs over a length of $\mathcal{O}(\epsilon\tau)$, since the balance in the temperature equation changes as $S_{\text{SiO}_2} \to 0$. In this narrow layer, the reaction rates balance the advective sensible heat and the external heating, while quartz and carbon still react, producing $G_{\text{SiO}}$. The cross-sectional area stabilises in this region such that $A = A_{\text{crit}}$ throughout. The interactions in this post-reaction transition zone are detailed in Sect. A.2. Subsequent to the transition layer, a final post-reaction regime emerges.

### 4.4 Post-reaction zone

After reaction (1) ceases, the kiln returns to a similar dominant balance as in the pre-heat zone. The heating source $Q$ balances the advective term in the temperature equation (61), causing significant further heating of the bed at a rate proportional to $\mathcal{O}(1/\epsilon\tau)$. The solid volume fractions and cross-sectional area are constant, fixed at the values they achieve at $x = x_{\text{crit}}$ when the hot zone ends. No gas is produced as no reactions can occur. As in the pre-heat zone, the dynamics are governed solely by a reduced temperature equation,

$$\frac{\mathrm{d}T}{\mathrm{d}x} = \frac{1}{\epsilon\tau u A_{\text{crit}}} Q, \tag{91}$$

which mirrors (69), but is scaled by the smaller cross-sectional area $A = A_{\text{crit}}$ in place of the inlet value $A_0 = 1$.

In the interests of energy efficiency, the kiln dimensions or $u$ should be chosen so that no further heating is applied after the end of the hot zone. Our asymptotic analysis above suggests that we impose $Q = 0$ for $x > x_{\text{crit}}$. Moreover, from a practical point of view, minimising the length of the post-reaction zone is desirable since no silicon carbide conversion occurs here. One way to achieve this is to choose the velocity $u$ such that $x_{\text{crit}} = 1$. This critical velocity is determined by

$$u_{\text{crit}} S^0_{\text{SiO}_2} = \int_{x_0}^{1} Q(\bar{x})\,\mathrm{d}\bar{x}, \tag{92}$$

by (88). We recall that $x_0$ depends on $u$ in (70), and so for general $Q$ (92) is an implicit relation.

The steady-state solution divides naturally into three axial zones (see Fig. 2), linked by thin $\mathcal{O}(\epsilon\tau)$ transition layers at $x = x_0$ and $x = x_{\text{crit}}$. In the pre-heat zone ($0 < x < x_0$), the quartz and carbon enter the bed cold. The Arrhenius term of $r_1$ is exponentially small, and so $r_2$, $F$, and $G_{\text{SiO}}$ are negligible. Both $A$ and the solid volume fractions remain at their inlet values. The temperature evolves from a balance between advective sensible heat and the imposed heating $Q$. The location $x_0$, at which $T \to 0$, follows from (70). Entering the hot zone ($x_0 < x < x_{\text{crit}}$), heating is almost consumed by

the endothermic quartz reduction, thus, $Q \sim r_1$ in this region. The associated gas evolution is determined through $F = 2Q$, in (81). Quartz is exhausted at $x = x_{\text{crit}}$ determined by (88), leaving an excess of carbon. Beyond $x_{\text{crit}}$, reactions cease through a second $\mathcal{O}(\epsilon\tau)$ transition layer, after which the post-reaction region reverts to a pre-heat-type balance. In the post-reaction zone we find $F = 0$, fixed composition of the solid materials, and that the temperature increases linearly due to external heating. To maximise efficiency, one would minimise the length of the post-reaction zone by choosing $u$ so that $x_{\text{crit}} = 1$.

### 4.5 Silicon carbide yield and carbon utilisation

We recall that the important metrics to maximise are $Y_{\text{sic}}$ and $U_{\text{c}}$ given by (66) and (67) respectively. Assuming that the kiln parameters are chosen so that reactions in the hot-zone are completed before the end of the kiln, $x_{\text{crit}} < 1$. Since no further reactions happen for $x > x_{\text{crit}}$, both $Y_{\text{sic}}$ and $U_{\text{c}}$ may equally be defined at $x = x_{\text{crit}}$ rather than at $x = 1$.

In the analysis thus far, we have taken the distinguished limit $\Gamma = O(1)$. We recall that $\Gamma$ is proportional to $k_2/k_1 r_c^0$, and so can be interpreted as the ratio between the reaction rates, accounting for temperature effects and particle-scale geometry. We now consider two sub-limits, of small and large $\Gamma$, representing slow and fast reaction kinetics.

#### 4.5.1 Slow reaction limit

In the slow reaction limit where $\Gamma \ll 1$, (75) reduces at leading-order to $G_{\text{sio}} = 0$ (since we have already found that $F = 2Q > 0$). As a consequence, $r_2 = 0$ and reaction (2) does not proceed. We do not create any silicon carbide in this limit. In this regime, the silicon carbide yield is $Y_{\text{sic}} = 0$, and the carbon utilisation is $U_{\text{c}} = 1/3$.

#### 4.5.2 Fast reaction limit

We now consider the more interesting limit of $\Gamma \gg 1$, which we interpret as reaction (2) having a much faster rate than reaction (1), so that reaction (2) is limited by reaction (1). To leading order, (75) reduces to $Ar_1 = Ar_2$, or equivalently $Ar_2 = Q$ by (77), and so the two reactions proceed at the same speed. Any silicon monoxide produced by reaction (1) is immediately consumed by reaction (2). We may now integrate (72) to find the volume fraction of carbon

$$S_{\text{c}} = \frac{1}{A}\left(S_{\text{c}}^0 - \frac{3\,\mathcal{C}_{\text{c}}}{u}\int_{x_0}^{x} Q(\bar{x})\,\mathrm{d}\bar{x}\right), \tag{93}$$

which is reminiscent of (90). Recall from the previous discussions that in this regime $S_{\text{c}}(x_{\text{crit}}) = 0$. Indeed, another way we can show this is by noting that (84) and (93) vary by a factor of $3\,\mathcal{C}_{\text{c}}$ (by (25)). With sufficient heating $Q$ the quartz and the carbon

are fully consumed at the same point, $x_{\text{crit}} \leq 1$, along the kiln. After this critical point

$$S_{\text{SiC}} = 1 - \phi_0. \tag{94}$$

We may perform a similar integration of (74) to show that after this same critical point $x_{\text{crit}}$ the cross-sectional area is

$$A = 1 + \frac{S^0_{\text{SiO}_2}(-1 - 3\,\mathcal{C}_{\text{C}} + \mathcal{C}_{\text{SiC}})}{1 - \phi_0}. \tag{95}$$

We have already shown that $S_{\text{C}}(1) = 0$ (by assuming sufficient heating $Q$ such that $x_{\text{crit}} \leq 1$), and so the carbon utilisation is $U_{\text{C}} = 1$. We now compute the yield. Substituting (94) and (95) into the definition of the yield (66), we obtain

$$Y_{\text{SiC}} = \frac{1}{\mathcal{C}_{\text{SiC}} S^0_{\text{SiO}_2}} \left(1 - \phi_0 - S^0_{\text{SiO}_2} - 3\,\mathcal{C}_{\text{C}} S^0_{\text{SiO}_2} + \mathcal{C}_{\text{SiC}} S^0_{\text{SiO}_2}\right). \tag{96}$$

Notice that

$$1 - \phi_0 - S^0_{\text{SiO}_2} - 3\,\mathcal{C}_{\text{C}} S^0_{\text{SiO}_2} = 0, \tag{97}$$

by our boundary conditions (24) and (25), and thus, $Y_{\text{SiC}} = 1$. Not only do we consume all of the quartz and carbon so that only silicon carbide is extracted from the kiln, but we achieve a perfect silicon carbide yield—no silicon is lost as silicon monoxide gas.

We note that our analysis in this subsection *did not* rely on the exact reaction kinetics chosen for reaction (2). Therefore, even if our assumed reaction kinetics do not precisely model the underlying physics and chemistry it is always the case that $Y_{\text{SiC}} \to 1$ when the associated dimensionless parameter $\Gamma \to \infty$.

## 5 Numerical solutions

We now consider the more general asymptotic regime described at the beginning of Sect. 4 where the dimensionless parameter $\delta \ll 1$, while all other parameters remain $\mathcal{O}(1)$. To close the system, we adopt the simplification that the external heat input is spatially uniform, and write $Q(x) = 1$. We seek a numerical solution to the reduced system (54)–(63), which consists of four partial differential equations and three algebraic constraints. The parameter $\delta$ represents the equilibration time scale of the gas phase. Consequently, it is natural that the three algebraic constraints arise from the three equations involving the gas dynamics. The system is implemented in Julia [45], and we solve the resulting differential-algebraic equations (DAE) with the `IDA` solver from the SUNDIALS suite [46], which is well-suited for DAE systems such as ours. The time integrations performed by `IDA` use variable-order, variable-coefficient backward differentiation formulas (BDF) [46].

An example of the numerical solution is shown in Fig. 3, using the parameter values listed in Table 3. The steady-state temperature profile is presented in Fig. 3a. For small

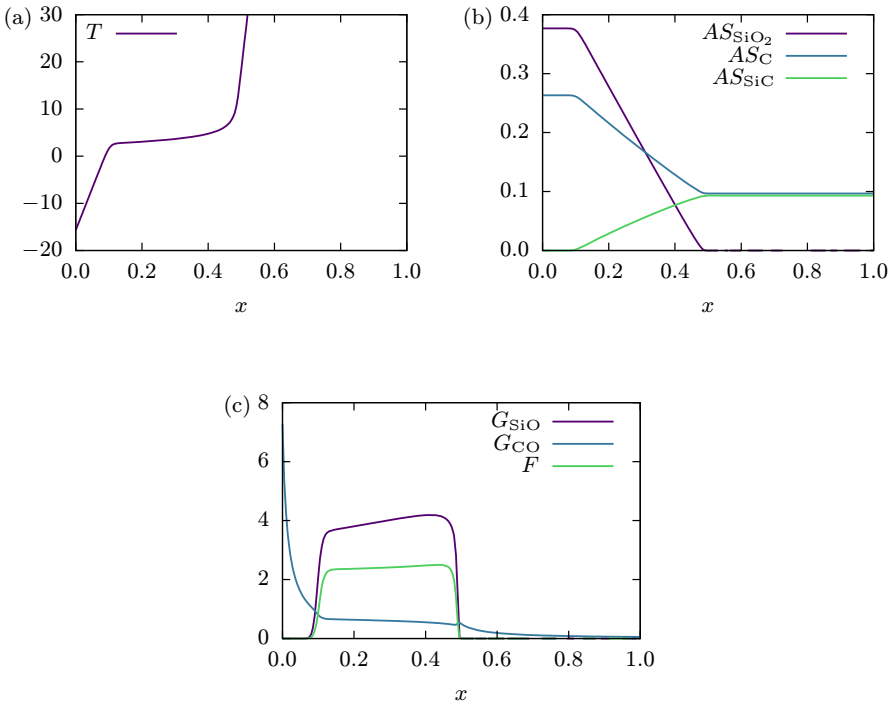


**Fig. 3** Numerical solution of the (dimensionless) steady-state system (54)–(63) using the parameter values found in Table 3 with $u = 1.0$, showing, as a function of position $x$ along the kiln, (a) the bed temperature, (b) the amount of each solid species (in the bed, cross-sectional area $A$), and (c) the concentrations $G$ of each gas species along with the total gaseous production flux $F$

values of $x$, we observe the expected pre-heating zone, in which the solid bed is brought to reaction temperature. In this region, the dominant balance in the temperature equation is between the advective transport term and the external heating source $Q$. Beyond this, the temperature plateaus in the hot zone, where the enthalpy of the reactions is balanced by the applied heating. For $x \geq x_{\text{crit}} \approx 0.5$, the reactions cease and we enter the post-reaction zone. The temperature once again rises due to the continued supply of heat—once again balancing advection. As expected from our asymptotic analysis, the temperature gradient in the post-reaction zone is steeper than in the initial pre-heating zone, owing to the reduced cross-sectional area of the reacted bed. The evolution of the solid-phase species is shown in Fig. 3b. In the pre-heating zone, the solid volume fractions remain constant since the reactions have not begun. Within the hot zone, we observe nearly linear consumption of quartz and carbon, alongside the linear formation of silicon carbide. Around $x = x_{\text{crit}}$, the quartz is fully consumed, halting further reactions. All solid phase profiles flatten beyond this point. In Fig. 3c we show the gas concentrations and the associated flux out of the bed. In the pre-heating zone, the concentration of silicon monoxide and gas flux are zero, while the concentration of carbon monoxide decreases due to the rising temperature. In the hot zone, the silicon monoxide concentration increases, while that of carbon monoxide

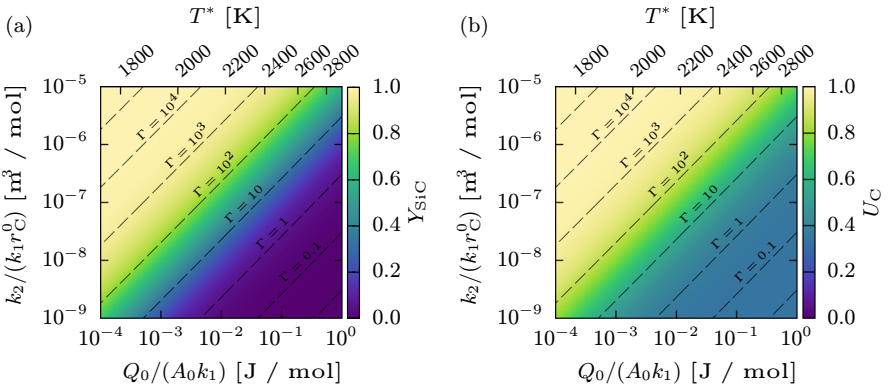


**Fig. 4** (a) Silicon carbide yield, given by (66), and (b) carbon utilisation, given by (67), obtained from the numerical solution of the system (54)–(63) as we vary the two key dimensional parameters (98), with $u = 1.0$

is fairly uniform. The gas flux out of the bed is also nearly uniform throughout this region, consistent with the approximately constant rate of solid consumption and the asymptotic behaviour in (81). In the post-reaction zone we find similar behaviour as in the pre-heat zone. The concentration of silicon monoxide and the gas flux are 0, while the concentration of carbon monoxide decreases due to the increasing temperature. For the baseline parameters listed in Table 3, we obtain a silicon yield of $Y_{\text{SiC}} = 0.4490$ and a carbon utilisation of $U_{\text{C}} = 0.6329$.

We now examine the effect of the dimensionless parameters on the silicon carbide yield and carbon utilisation. As discussed in Sect. 3.3, all dimensionless parameters in the model are governed by the two key dimensional groupings

$$\frac{Q_0}{A_0 k_1}, \quad \frac{k_2}{k_1 r_{\text{c}}^0}, \tag{98}$$

and the velocity $u$. The first of the dimensional groups represents the ratio of externally supplied heat to the axial rate of reaction (1), and determines the intrinsic temperature $T^*$. The second group expresses the relative rate of the silicon carbide reaction (2) to that of the quartz reaction. Together these two ratios define the dimensionless parameter $\Gamma$. While $k_1$ and $k_2$ in practice are fixed (though their values are not precisely known), both $Q_0$ and $r_{\text{c}}^0$ can be varied over orders of magnitude and, to a lesser extent, we can vary $A_0$. Figure 4 presents the silicon carbide yield and carbon utilisation as we sweep through these two parameter groupings with $u = 1.0$. We observe that decreasing $Q_0/(A_0 k_1)$ or increasing $k_2/(k_1 r_{\text{c}}^0)$ improves both yield and utilisation. A smaller $Q_0/(A_0 k_1)$ reduces the rate of the quartz reaction (1), leading to less silicon monoxide escaping via the gas channel and more reacting with carbon to form silicon carbide. Similarly, a larger $k_2/(k_1 r_{\text{c}}^0)$ directly increases the rate of the silicon carbide reaction (2)—boosting yield. These results are governed almost entirely by the value of $\Gamma$ (shown by dashed lines in Fig. 4). Although varying $Q_0/(A_0 k_1)$ affects $T^*$ and therefore the parameters $\tau$, $\sigma$, $\epsilon$, and $\mathcal{T}$, we are focused on a narrow temperature

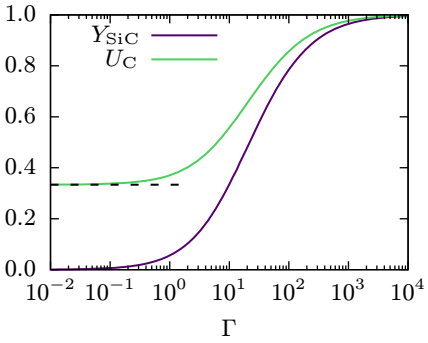


**Fig. 5** Silicon carbide yield, given by (66), and carbon utilisation, given by (67), obtained from the numerical solution of the system (54)–(63) as we vary Γ, with $u = 1.0$

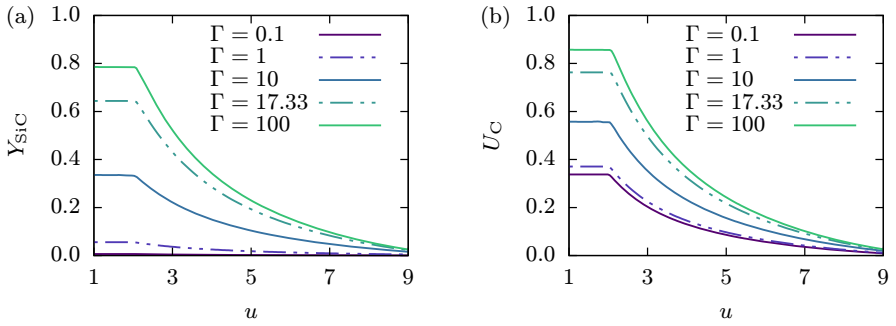


**Fig. 6** (a) silicon carbide yield, given by (66), and (b) carbon utilisation, given by (67), obtained from the numerical solution of the system (54)–(63) as we vary $u$ for various values of Γ

range to avoid triggering additional reactions, thereby limiting the range of values that these dimensionless parameters can take. In contrast, Γ varies linearly with $k_2/(k_1 r_c^0)$, which can span orders of magnitude. Thus, the dynamics of the system are controlled by Γ (and, to a weaker extent, by $u$, which we examine shortly).

Since the system dynamics are governed almost entirely by Γ, we now examine the effect of this parameter in more detail. In Fig. 5, we plot the silicon carbide yield and carbon utilisation as functions of Γ, holding all other parameters fixed at the values listed in Table 3. This corresponds to a vertical slice through Fig. 4 at $T^* = 2182.4$ K. As previously observed in Fig. 4, both the yield $Y_{SiC}$ and the utilisation $U_C$ increase monotonically with Γ. In the limit $\Gamma \to \infty$, we have $Y_{SiC} \to 1$ and $U_C \to 1$. Conversely, as $\Gamma \to 0$, the yield tends to 0, while the utilisation approaches $U_C \to \frac{1}{3}$. In this regime, the critical position $x_{crit} < 1$, indicating that the quartz has fully reacted before the outlet. Consequently, one third of the initial carbon is consumed by the quartz reaction, (1).

Up to this point, we have only considered the case $u = 1.0$. In Fig. 6, we show the silicon carbide yield and carbon utilisation as $u$ is varied, for several values of Γ. The results indicate that both metrics remain constant for $u \lesssim 2.05$, beyond which they begin to decay sharply to 0. Recall we predicted a critical $u$ value in (92). For $Q = 1$

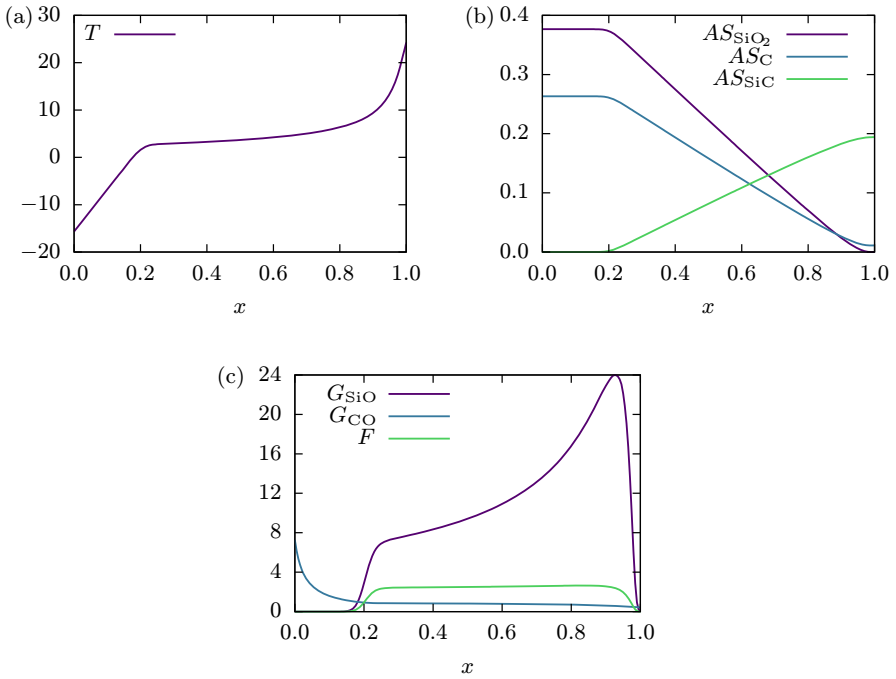


**Fig. 7** Numerical solution of the system (54)–(63) using the parameter values found in Table 3 with $\Gamma = 500$ and $u = 2$, showing, as a function of position $x$ along the kiln, (a) the bed temperature, (b) the amount of each solid species (in the bed, cross-sectional area $A$), and (c) the concentrations $G$ of each gas species along with the total gaseous production flux $F$

we find that

$$u_{\text{crit}} \approx \left(S^0_{\text{SiO}_2} + \tau\,(1-\mathcal{T})\right)^{-1}, \tag{99}$$

$$\approx 2.15. \tag{100}$$

The critical speed we recover numerically is close to what is predicted from the asymptotics. The numerical result is slightly lower, however, since we lose some thermal energy via the gas flux $F$ in the numerical solution, which we neglected in the asymptotics. Indeed, the two critical speeds vary by $\mathcal{O}(\sigma)$. For speeds below the critical threshold, the quartz is fully consumed before the end of the reactor, resulting in a post-reaction zone where no further reaction occurs (i.e., $x > 0.5$ in Fig. 3). Increasing $u$ has no impact on the overall yield or utilisation, but shortens the length of the post-reaction zone. At the critical value, the quartz is fully reacted precisely at the outlet. When $u$ exceeds this value, the quartz does not fully react within the length of the reactor, leading to a significant drop in efficiency. As $u \to \infty$, both metrics tend to 0. Notice that the expression for $u_{\text{crit}}$ in (99) is independent of $\Gamma$, which we confirm numerically in Fig. 6: the shape of the profiles remains unchanged while varying $\Gamma$—only the maximum achievable yield and utilisation are affected.

Now that we have developed a clearer understanding of the system dynamics, we consider case with $\Gamma = 500$ and $u = 2.0$. We show the solution in Fig. 7. We observe that the length of the pre-heating zone has doubled, occurring in the region $x \leq 0.2 \approx u\tau$. As in the previous case, we find linear consumption of quartz and carbon and corresponding linear production of silicon carbide. The quartz is fully consumed just before the end of the reactor, and, owing to the large value of $\Gamma$, the carbon is nearly fully consumed as well. Consequently, this set-up yields significantly more silicon carbide than the previous case. With this set of parameters we recover a silicon carbide yield of 0.9364 and a carbon utilisation of 0.9581. The behaviour of the concentration of carbon monoxide $G_{\mathrm{CO}}$ and the flux out of the bed $F$ remains qualitatively unchanged. The silicon monoxide concentration profile $G_{\mathrm{SiO}}$ exhibits a similar shape, but with a larger dimensionless concentration, reflecting the increased reactivity associated with larger $\Gamma$.

## 6 Conclusions

We have developed a one-dimensional steady-state model to study silicon carbide production in a rotary kiln. The model captures essential physical and chemical processes, including solid bed motion, solid-phase heat transfer, gas flow, and a simplified set of chemical reactions. A key aim was to maintain a simple and computationally efficient framework suitable for easy interpretation and broad-brush optimisation of kiln design and operating parameters. Several simplifying assumptions were made, including that the granular bed is well mixed due to rotation, the bed moves down the kiln at a uniform velocity, and that the gas pressure remains close to atmospheric throughout. Despite these idealisations, the model yields solutions that appear physically plausible and provide useful insight into the process. Important future work will need to compare the model solutions with experimental measurements from prototype rotary-kiln silicon carbide reactors, as these are developed. The structure of the model also allows for straightforward inclusion of more complex effects, such as additional reactions or pressure-driven gas flow.

A central concern motivating this study was the potential for silicon monoxide gas, generated via the reduction of quartz, to escape the bed before reacting with carbon to form silicon carbide. The model confirms that high silicon carbide yields require a large value of a key dimensionless group, $\Gamma$, representing the ratio of the rate of silicon carbide formation to the rate of quartz reduction. We found that silicon carbide yield increases monotonically with this dimensionless parameter. This suggests that reaction (2) must proceed significantly faster than reaction (1) to capture the silicon monoxide gas before it is lost.

Our findings are consistent with experimental studies in the literature. Li et al. [10] noted that conversion depends both on the rate that silicon monoxide is produced and on the rate at which it is subsequently captured by carbon. When silicon carbide formation is sufficiently fast, essentially all of the generated silicon monoxide is captured. More broadly, studies have found that increasing reactant surface area by reducing particle size improves reaction rates [10, 13]. This aligns with our interpretation of $\Gamma$ as a relative kinetic measure. Similarly, Biernacki et al. [9] found that diffusion path

lengths within the porous bed, and therefore particle size, significantly influence the observed rate.

One valuable result from both the asymptotics and numerics was the emergence of a critical solid velocity. The critical velocity is such that the quartz is fully consumed at the outlet of the reactor. No interesting dynamics or silicon carbide conversion can occur after the quartz has been consumed. It is beneficial to have the consumption of the quartz to occur near the outlet. Both the asymptotics and numerics showed that the critical dimensionless velocity is slightly larger than 2, which in dimensional form is

$$u_{\text{crit}} \approx 2\frac{Q_0 L M_{\text{SiO}_2}}{A_0 \Delta H_1 \rho_{\text{SiO}_2}}. \tag{101}$$

We recommend choosing the diameter, rotation speed, and inclination angle of the kiln so that the solid velocity closely matches (101). Moreover, we recommend a solid velocity (and matching critical velocity) that is as large as reasonably possible. Increasing the velocity increases the flux of the silicon carbide out of the kiln, thus increasing the amount of silicon carbide that can be produced in a given time. This is a particularly useful industrial metric—the faster silicon carbide is produced the more profitable the process.

If the rotary kiln configuration proves viable for silicon carbide production, the modelling framework developed here offers a promising tool for rapid exploration and optimisation of key design variables, such as heating profiles, kiln geometry, and feedstock properties.

Our modelling framework may additionally be extended to relax some of our simplifying assumptions, or to include additional physical processes. We neglected any explicit model of the gas flow and heat transfer in the channel above the bed. Future work should explore a coupled system where the central channel dynamics interact with the bed through both thermal and mass exchange. Such coupling may be especially relevant in the pre-heat region. Moreover, the model developed omits any possible condensation reactions that may occur at the lower temperatures in the pre-heat zone. Silicon monoxide is unstable at low temperatures, and can break down by $2\,\text{SiO}(g) \rightarrow \text{SiO}_2(s) + \text{Si}(l)$, or undergo the reversal of reaction (1) in the presence of carbon monoxide. These reactions could allow recapture of quartz upstream and reduce the silicon monoxide loss. The silicon carbide yield might be increased slightly by including these reactions. However, these reactions are complex kinetically since they become faster as temperature *decreases*.

In our modelling and analysis we assumed the carbon particles were spherical and that all particles at a particular location and time were the same size. In reality, both of these assumptions are likely to (at least partially) break down. Carbon particles typically have rough and porous surfaces, and follow a particle size distribution. A different proportionality constant between characteristic size and volume or surface area may be more appropriate to model the consumption. Incorporating particle size distribution into the model complicates the modelling and analysis, but is likely to be fruitful. One possible framework for modelling reactive flows with particle size dependence is presented in [47].

We assumed that the bed is well mixed in each cross-section and that all variation is along the axial direction. However, depending on the form of the feedstock, this assumption may not hold. If the material is fed as individual particles rather than agglomerates or pellets, then density differences between quartz, carbon, and silicon carbide may lead to vertical separation in the rotary kiln. This is particularly relevant since the degree of mixing of the raw materials can strongly influence reaction rate [48]. Moreover, we neglect any axial mixing along the bed. In practice, mixing along the length of the kiln may be significant. Finnie et al. [49] have showed that such mixing can be captured by an effective diffusion term in the axial direction. Future modelling could incorporate this additional term to assess its impact on silicon carbide production.

In the present model, the external heat flux is specified a priori. A promising extension is to pose an inverse or control problem, where the heat flux is chosen to achieve a desired temperature profile—for instance, uniform in the hot zone. This could allow for better control of the reaction zone, improve yield, and reduce overheating of the materials. Moreover, practical constraints on the heating profile will need to be included based on the choice of external heat source.

Another instructive extension is to include off-gassing in the pre-heat region. Depending on the material preprocessing, the raw feedstock may contain significant water content or other volatiles. These components must evaporate in the pre-heat zone. Owens et al. [30] found that water vaporisation can substantially delay heating and alter the temperature profile in rotary kilns. Understanding the volatile mass fractions and latent heat demands would provide a more complete thermal model and may be necessary for kiln optimisation.

The insights gained here form a foundation for understanding and optimising rotary kiln design and operation for silicon carbide production. Our model serves as a starting point for more detailed investigations that incorporate additional physical mechanisms and industrial constraints.

**Acknowledgements** The authors would like to thank Aasgeir Valderhaug, Antoine Autruffe, and Sergey Bublik, Elkem ASA, as well as Anthony Bonfils and the rest of the participants at the 186th European Study Group with Industry (ESGI), where this problem was first presented [50].

**Author contributions** All authors contributed to model development and analysis. B.M. computed numerical solutions. All authors contributed to writing and reviewing the manuscript.

**Funding** EKL is grateful for funding from the Leverhulme Trust via an Early Career Fellowship ECF-2024-172.

**Data availability** No datasets were generated or analysed during the current study.

## Declarations

**Conflict of interest** The authors declare no conflict of interest.

## A Dynamics in transition zones

The transitions zones are thin layers, within which, the temperature evolves rapidly to transition smoothly between adjacent regions. We first discuss the transition between the pre-heat and hot zone in Sect. A.1, while the transition from hot zone to post-reaction zone is discussed in Sect. A.2.

### A.1 Pre-heat transition zone

As the temperature rises from large negative values in the pre-heat zone to $\mathcal{O}(1)$ in the hot zone, the balance in the problem changes. In the temperature equation (43), the heat of reaction terms become $\mathcal{O}(1)$ and balance the advective sensible heat and the external heating for $(x - x_0) = \mathcal{O}(\epsilon\tau)$, where the transition point $x_0$ is defined in (70).

Substituting the scaled spatial variable

$$x - x_0 = \epsilon\tau\widehat{x}, \tag{102}$$

the advective terms become $\mathcal{O}(1/\epsilon\tau)$ in the quartz, carbon, and cross-sectional area equations, (54), (55), and (58), while the other terms are $\mathcal{O}(1)$ and thus negligible at leading-order. Consequently, the solid volume fractions and the cross-sectional area remain constant throughout this region, as in the pre-heat zone, retaining their inlet values. That is, $A = 1$, $S_{\mathrm{SiO_2}} = S^0_{\mathrm{SiO_2}}$, and $S_{\mathrm{C}} = S^0_{\mathrm{C}}$ in the pre-heat transition zone.

With constant solid volume fractions, the reaction rate $r_1$ is a function of temperature alone, and is given by

$$r_1 = \mathrm{e}^T S^0_{\mathrm{SiO_2}} S^0_{\mathrm{C}}, \tag{103}$$

recalling that $\epsilon T \ll 1$ in this region since $T = \mathcal{O}(1)$. This allows the temperature equation (61) to decouple from the other variables and reduce to the simple leading-order equation

$$u\frac{\mathrm{d}T}{\mathrm{d}\widehat{x}} = Q - r_1, \tag{104}$$

after performing the change of variable. The flux of gases from the bed (60) reduces to $F = 2r_1$, indicating that the gas escaping from the bed is governed by the reaction rate $r_1$. Inserting $F = 2r_1$ into (59), and rearranging, we find that

$$G_{\mathrm{SiO}} = \frac{\Gamma r_1}{2r_1 + \Gamma\phi_0(S^0_{\mathrm{C}})^{2/3}}. \tag{105}$$

The gas concentration $G_{\mathrm{CO}}$ can be recovered from the ideal gas law (62)

$$G_{\mathrm{CO}} = 1 - \frac{1}{\Gamma} G_{\mathrm{SiO}}. \tag{106}$$

This thin transition layer captures the abrupt decrease in temperature gradient at $x_0$. The reaction rates control the production of gas and combine with external heating to contribute to the temperature evolution.

### A.2 Post-reaction transition zone

The post-reaction zone occurs when the volume fraction of quartz is small. In this zone the temperature increases rapidly, which can be seen from the divergence of (80). As with the pre-heat transition zone, this transition occurs over a narrow region of $\mathcal{O}(\epsilon\tau)$, centred about $x_{\mathrm{crit}}$ defined by (88). The key difference between the dynamics in this layer and the pre-heat transition zone is that here we achieve a dominant balance in the quartz equation. Additionally, we must also scale the temperature since it is no longer $\mathcal{O}(1)$.

We scale into this transition layer via the spatial and quartz transformations

$$x - x_{\mathrm{crit}} = \epsilon\tau\widehat{x}, \quad S_{\mathrm{SiO_2}} = \epsilon\tau\widehat{S}_{\mathrm{SiO_2}}, \tag{107}$$

for a dominant balance between the advective sensible heat, the external heating, and the reaction term. Furthermore, as the volume fraction of quartz is non-constant in this layer we require the dominant balance in the quartz volume fraction equation (54) to be between the advective and reaction terms. Substituting (107) into (54), we find that $\exp(T) \sim 1/\epsilon\tau$. We now introduce the scaled temperature $\widehat{T}$ such that $\exp\left(\widehat{T}\right) = \mathcal{O}(1)$, and rearrange to obtain that the temperature scaling within this layer is

$$T = -\log(\epsilon\tau) + \widehat{T}. \tag{108}$$

Beginning with the area equation (58) we perform these change of variables to find

$$(1-\phi_0)u\frac{\mathrm{d}A}{\mathrm{d}\widehat{x}} = \epsilon\tau A\Big( -(1+\mathcal{C}_{\mathrm{c}})\mathrm{e}^{\widehat{T}}\widehat{S}_{\mathrm{SiO_2}}S_{\mathrm{c}} + (\mathcal{C}_{\mathrm{SiC}} - 2\,\mathcal{C}_{\mathrm{c}})r_2\Big). \tag{109}$$

We make two crucial observations. To leading-order, the cross-sectional area is constant, and the correction is of $\mathcal{O}(\epsilon\tau)$. Thus, $A = A_{\mathrm{crit}} + \epsilon\tau A_1 + \cdots$. Similarly, the carbon volume fraction is $\mathcal{O}(1)$ in this region. Substituting the scaled variables into (55) we obtain

$$u\frac{\mathrm{d}}{\mathrm{d}\widehat{x}}(AS_{\mathrm{c}}) = -\epsilon\tau\mathcal{C}_{\mathrm{c}}A\left(\mathrm{e}^{\widehat{T}}\widehat{S}_{\mathrm{SiO_2}}S_{\mathrm{c}} + 2r_2\right), \tag{110}$$

and so the volume fraction of carbon to leading-order is constant at $S_{\mathrm{c}}^{\mathrm{crit}}$.

With this in mind, the temperature equation, to leading-order, becomes

$$u A_{\text{crit}} \frac{\mathrm{d}\widehat{T}}{\mathrm{d}\widehat{x}} = Q - A_{\text{crit}} \mathrm{e}^{\widehat{T}} \widehat{S}_{\text{SiO}_2} S_{\text{c}}^{\text{crit}}, \tag{111}$$

which is analogous to (104). We note that the correction term of $\widehat{T}$ is of $\mathcal{O}(\tau)$, *not* $\mathcal{O}(\epsilon\tau)$ as one might expect. The leading-order equation for the volume fraction of quartz is

$$u \frac{\mathrm{d}\widehat{S}_{\text{SiO}_2}}{\mathrm{d}\widehat{x}} = -\mathrm{e}^{\widehat{T}} \widehat{S}_{\text{SiO}_2} S_{\text{c}}^{\text{crit}}. \tag{112}$$

We note that $\widehat{S}_{\text{SiO}_2} \to 0$ as $\widehat{x} \to \infty$, which matches with the post-reaction zone.

The gas flux from the bed is $F = 2A_{\text{crit}}\widehat{r}_1$, while the gas concentration of silicon monoxide evolves at leading-order according to the algebraic constraint

$$G_{\text{SiO}} = \frac{\Gamma \widehat{r}_1}{2\widehat{r}_1 + \Gamma\phi_0 \left( \dfrac{\left(S_{\text{c}}^{\text{crit}}\right)^2}{A_{\text{crit}}} \right)^{1/3}}, \tag{113}$$

where $\widehat{r}_1 = \exp(\widehat{T})\widehat{S}_{\text{SiO}_2} S_{\text{c}}^{\text{crit}}$. Both the gas flux and silicon monoxide production depend on the temperature and quartz volume fraction.

## References


1. Carter CB, Norton MG (2013) Ceramic materials: science and engineering. Springer, New York
2. Casady JB, Johnson RW (1996) Status of silicon carbide (SiC) as a wide-bandgap semiconductor for high-temperature applications: a review. Solid-State Electron 39(10):1409–1422
3. Snead LL, Nozawa T, Ferraris M, Katoh Y, Shinavski R, Sawan M (2011) Silicon carbide composites as fusion power reactor structural materials. J Nucl Mater 417(1–3):330–339
4. Saddow S (2022) Silicon carbide technology for advanced human healthcare applications. Micromachines 13(3):346
5. Ou H (2024) Silicon carbide, the next-generation integrated platform for quantum technology. Light Sci Appl 13(1):219
6. Acheson EG (1895) Production of artificial crystalline carbonaceous materials. US Patent Reissue 11473
7. Kumar PV, Gupta GS (2002) Study of formation of silicon carbide in the Acheson process. Steel Res 73(2):31–38
8. Lee JG, Miller PD, Cutler IB (1977) Carbothermal reduction of silica. Reactivity of solids. Springer, New York, pp 707–711
9. Biernacki J, Wotzak G (1989) Thermogravimetric study of the C + $SiO_2$ reaction. J Therm Anal 35(5):1651–1667
10. Li F, Tangstad M, Ringdalen E (2018) Carbothermal reduction of quartz and carbon pellets at elevated temperatures. Metall Mater Trans B 49B:1078–1088
11. Weimer AW, Nilsen KJ, Cochran GA, Roach RP (1993) Kinetics of carbothermal reduction synthesis of beta silicon carbide. Am Inst Chem Eng J 39(3):493–503
12. Tian J, Wei K, Deng X, Ma W (2024) A study of the effect of quartz-to-cristobalite transformation on SiC generation in metallurgical-grade silicon production. SILICON 16(7):3155–3164

13. Agarwal A, Pal U (1999) Influence of pellet composition and structure on carbothermic reduction of silica. Metall Mater Trans B 30(2):295–306
14. Blumenthal JL, Santy MJ, Burns EA (1966) Kinetic studies of high-temperature carbon-silica reactions in charred silica-reinforced phenolic resins. Am Inst Aeronautics Astronautics J 4(6):1053–1057
15. Khalafalla SE, Haas LA (1972) Kinetics of carbothermal reduction of quartz under vacuum. J Am Ceram Soc 55(8):414–417
16. Klinger N, Strauss EL, Komarek KL (1966) Reactions between silica and graphite. J Am Ceram Soc 49(7):369–375
17. Lee JG, Cutler IB (1975) Formation of silicon carbide from rice hulls. Am Ceram Soc Bull 54(2):195–198
18. Wiik K (1990) Kinetics of reactions between silica and carbon. PhD thesis, The Norwegian Institute of Technology, Trondheim, Norway
19. Li F (2017) SiC production using $SiO_2$ and C agglomerates. PhD thesis, Norwegian University of Science and Technology, Trondheim, Norway
20. Lindgaard H (2015) High temperature decomposition of methane on quartz pellets. Master's thesis, Norwegian University of Science and Technology, Trondheim, Norway
21. Metherall B, Breward CJW, Please CP, Oliver JM, Sloman BM (2023) Modelling the reduction of quartz in a quartz-carbon pellet. J Eng Math 141(1):4
22. Metherall B, Breward CJW, Please CP, Oliver JM (2025) Multiphase modelling and optimisation of silicon carbide production (submitted)
23. Andrews J, Azemar A, Bhattacharya A, Egan C, Lacey A, Metherall B, Ryan N (2024) Mathematical modelling of a silicon carbide (SiC) pilot furnace. Math Industry Rep
24. Bisulandu B-JRM, Huchet F (2023) Rotary kiln process: an overview of physical mechanisms, models and applications. Appl Therm Eng 221:119637
25. Mellmann J (2001) The transverse motion of solids in rotating cylinders–forms of motion and transition behavior. Powder Technol 118(3):251–270
26. Boateng AA, Barr PV (1996) A thermal model for the rotary kiln including heat transfer within the bed. Int J Heat Mass Transf 39(10):2131–2147
27. Liu H, Yin H, Zhang M, Xie M, Xi X (2016) Numerical simulation of particle motion and heat transfer in a rotary kiln. Powder Technol 287:239–247
28. Witt PJ, Sinnott MD, Cleary PW, Schwarz MP (2018) A hierarchical simulation methodology for rotary kilns including granular flow and heat transfer. Miner Eng 119:244–262
29. Zhang Z, Liu Y, Zhao X, Xiao Y, Lei X (2019) Mixing and heat transfer of granular materials in an externally heated rotary kiln. Chem Eng Technol 42(5):987–995
30. Owens WD, Silcox GD, Lighty JS, Deng XX, Pershing DW, Cundy VA, Leger CB, Jakway AL (1991) Thermal analysis of rotary kiln incineration: comparison of theory and experiment. Combust Flame 86(1–2):101–114
31. Brennen CE (2005) Fundamentals of multiphase flow. Cambridge University Press, Cambridge
32. Jenike AW, Shield RT (1959) On the plastic flow of Coulomb solids beyond original failure. J Appl Mech 26(4):599–602
33. Nguyen TV, Brennen C, Sabersky RH (1979) Gravity flow of granular materials in conical hoppers. J Appl Mech 46(3):529–535
34. Luckins EK, Oliver JM, Please CP, Sloman BM, Van Gorder RA (2022) Modelling and analysis of an endothermic reacting counter-current flow. J Fluid Mech 949:21
35. Sloman BM, Please CP, Van Gorder RA (2019) Homogenization of a shrinking core model for gas-solid reactions in granular particles. SIAM J Appl Math 79(1):177–206
36. Szekely J, Evans JW, Sohn HY (1976) Gas-solid reactions. Academic Press Inc, New York
37. Yagi S, Kunii D (1955) Studies on combustion of carbon particles in flames and fluidized beds. Symp (Int) Combust 5(1):231–244
38. Krstic VD (1992) Production of fine, high-purity beta silicon carbide powders. J Am Ceram Soc 75(1):170–174
39. Meija J, Coplen TB, Berglund M, Brand WA, Bièvre PD, Gröning M, Holden NE, Irrgeher J, Loss RD, Walczyk T, Prohaska T (2016) Atomic weights of the elements 2013 (IUPAC Technical Report). Pure Appl Chem 88(3):265–291
40. NIST–JANAF (2025) NIST–JANAF thermochemical tables
41. Kadkhodabeigi M (2011) Modeling of tapping processes in submerged arc furnaces. PhD thesis, Norwegian University of Science and Technology, Trondheim, Norway

42. Berryman JG (1983) Random close packing of hard spheres and disks. Phys Rev A 27(2):1053–1061
43. Liu XY, Specht E (2006) Mean residence time and hold-up of solids in rotary kilns. Chem Eng Sci 61(15):5176–5181
44. Metherall B (2024) Modelling chemical and transfer processes in a silicon carbide reactor. PhD thesis, University of Oxford, Oxford
45. Bezanson J, Edelman A, Karpinski S, Shah VB (2017) Julia: a fresh approach to numerical computing. SIAM Rev 59(1):65–98
46. Hindmarsh AC, Brown PN, Grant KE, Lee SL, Serban R, Shumaker DE, Woodward CS (2005) SUNDIALS: suite of nonlinear and differential/algebraic equation solvers. ACM Trans Math Softw 31(3):363–396
47. González-Fariña R (2020) Modelling the mechanisms of microsilica particle formation and growth. PhD thesis, University of Oxford, Oxford
48. Koc R, Cattamanchi SV (1998) Synthesis of beta silicon carbide powders using carbon coated fumed silica. J Mater Sci 33:2537–2549
49. Finnie GJ, Kruyt NP, Ye M, Zeilstra C, Kuipers JAM (2005) Longitudinal and transverse mixing in rotary kilns: a discrete element method approach. Chem Eng Sci 60(15):4083–4091
50. Metherall B, Peschka D, Brosa Planella F, Iqbal A, Luckins E, Nazari N, Neff A, Plato L, Please C, Śliwiński M (2025) Mathematical modelling and optimisation of silicon carbide production in a rotary kiln reactor. Math Industry Rep (submitted)